Chapter 3
Preferential Oxidation of Carbon Monoxide in Hydrogen-Rich Streams over CuO/CeO_2 Catalysts: How Nano (and Subnano) Structure Affects Catalytic Activity and Selectivity

Almerinda Di Benedetto, Gianluca Landi, and Luciana Lisi

Abbreviations

(HR-)TEM	(High-resolution) transmission electron microscopy
(MW)CNT	(Multiwall) carbon nanotubes
(R)GO	(Reduced) Graphene oxide
[Bmim][BF_4]	1-Butyl-3-methylimidazolium tetrafluoroborate
BET	Brunauer-Emmet-Teller
BTC	1,3,5-Benzene-tricarboxylate
CO-PROX	Carbon monoxide preferential oxidation
CO-SMET	Carbon monoxide selective methanation
EDTA	Ethylenediaminetetraacetic acid
H_2-TPR	Hydrogen temperature programmed reduction
IL	Ionic liquid
MW	Microwave
NC	Nanocubes
NF	Nanofibers
NP	Nanoparticles
NR	Nanorods
NS	Nanospheres
PEM-FC	Proton exchange membrane fuel cell
SACOP	Silica aquagel coprecipitation
SFRD	Supercritical fluid reactive deposition

A. Di Benedetto
Dipartimento di Ingegneria Chimica, dei Materiali e della Produzione Industriale, University of Naples Federico II, Naples, Italy

G. Landi (✉) · L. Lisi
Institute of Sciences and Technologies for Sustainable Energy and Mobility CNR, Naples, Italy
e-mail: gianluca.landi@cnr.it

M. Piumetti, S. Bensaid (eds.), *Nanostructured Catalysts for Environmental Applications*, https://doi.org/10.1007/978-3-030-58934-9_3

TOF	Turnover frequency
TWC	Three way catalyst
WGS	Water gas shift
XPS	X-ray photoelectron spectroscopy
XRD	X-ray diffraction

3.1 Introduction

The need of green, renewable, transportable, and storable fuel is nowadays commonly accepted. In this context, hydrogen represents an ideal energy vector; it can be produced from several sources, such as solar, wind, biomass, and biogas, by different processes, such as electrolysis [1–3], reforming [4–7], thermochemical splitting [8, 9], photoelectrochemical splitting [10], etc. Moreover, hydrogen can be reacted with captured carbon dioxide to produce both fuels and fine chemicals.

The interest toward hydrogen as a fuel has been increased together with the development of proton exchange membrane fuel cells (PEM-FCs). PEM-FCs directly convert hydrogen and oxygen into water vapor and electricity; they show high efficiency, low operating temperature, and no moving parts, and are a mature technology [11]. Hydrogen streams produced by renewable and/or fossil fuel conversion (i.e., reforming, gasification, pyrolysis, etc.,) also contain CO, CO_2, and H_2O in different ratios. The hydrogen content is generally increased by one or two water gas shift (WGS) stages, according to Eq. (3.1).

$$CO + H_2O \leftrightarrow CO_2 + H_2 \tag{3.1}$$

Due to thermodynamic constraints, the CO concentration cannot be lowered below 0.5–2 vol.%. However, PEM-FCs suffer from poisoning by carbon monoxide even at very low concentration ($\leq$100 ppm); as a matter of fact, CO strongly adsorbs onto Pt active sites of the PEM-FC anode [11]. This means that a purification stage is necessary.

Two main processes have been proposed in order to convert CO: selective methanation [CO-SMET; (Eq. 3.2)] and preferential oxidation [CO-PROX; (Eq. 3.3)] [12–14].

$$CO + 3H_2 \leftrightarrow CH_4 + 2H_2O \tag{3.2}$$

$$CO + 0.5O_2 \rightarrow CO_2 \tag{3.3}$$

Both of them present pros and cons. Both reactions are exothermic ($\Delta H_{CO\text{-}SMET} \approx -206$ kJ/mol$_{CO}$; $\Delta H_{CO\text{-}PROX} \approx -283$ kJ/mol$_{CO}$), and thus, no external heating is required (but heat management is needed). Both reactions compete with undesired reactions; CO_2 methanation and reverse WGS can occur in parallel with CO-SMET,

while H_2 combustion and reverse WGS can occur in parallel with CO-PROX. H_2 consumption, even if undesired, is unavoidable in both processes. During CO-SMET, 3 moles of hydrogen per mole of carbon monoxide are consumed even at 100% selectivity (i.e., no CO_2 consumption by methanation or reverse WGS occurs). CO-PROX cannot be carried out under stoichiometric conditions, generally O_2 excess being necessary. However, oxygen cannot be fed to the Pt anode, because hydrogen should be directly burned without the production of protons to be transferred to the cathode side. Therefore, during CO-PROX, H_2 consumption is directly related to O_2 excess [15]. The typical equivalence ratio (λ; it corresponds to the ratio between the actual O_2/CO ratio and the stoichiometric one) is 2; this means that 1 mole of hydrogen per mole of carbon monoxide is consumed at complete CO and O_2 conversions. Accordingly, CO-PROX is characterized by a lower H_2 loss than CO-SMET.

On the other hand, O_2 supply for CO-PROX occurs via air addition, related to safety issues in the mixer; moreover, the low but not negligible hydrogen dilution with nitrogen is to be considered as a con absent for CO-SMET.

A definitive preference between CO-PROX and CO-SMET has not yet been defined; however, some prototype systems have been developed with one or more CO-PROX stages to purify the hydrogen stream [16–19].

The first paper on CO-PROX was published in 1922 [20], followed by other two papers in 1930 [21, 22]. In these works, CO-PROX was suggested as the purification stage of hydrogen streams for the Haber process. As is known, CO-PROX is not used in the Haber process and, thus, the interest toward this reaction dramatically dropped.

Fundamental studies on the platinum activity toward CO and H_2 oxidation [23–25] led to renewed interest toward CO-PROX [26]. As is known, platinum can be considered as an intrinsic preferential CO oxidation catalyst due to the strong CO adsorption at low temperature, which is also the reason for the high sensitivity of PEM Pt anodes to low CO partial pressures in the H_2 streams.

Starting from these works, the number of papers related to CO-PROX significantly increased, as shown in Fig. 3.1. Obviously, the increase was strictly related to the development of low-temperature PEM-FC.

Catalysts for preferential oxidation of carbon monoxide should show (1) good activity toward CO oxidation, (2) high selectivity (i.e., hydrogen oxidation rate should be lower than CO oxidation rate), (3) resistance to the inhibiting effect of carbon dioxide and water vapor (unavoidable in reformate streams), and (4) long life-time. Noble metal-based catalysts were first studied and are still of interest [27–33]. Their performance toward CO-PROX was also reviewed [12, 34]. In addition to platinum, gold nanoparticles were also proposed for CO-PROX showing interesting activity, selectivity, and resistance to the inhibiting effect of CO_2 and H_2O [27, 35–40]. A review of the most interesting results was published by Lakshmanan et al. [41].

Transition metal oxides, mainly supported on ceria, represent the last class of catalysts proposed for CO-PROX. Despite several attempts, copper oxide supported on ceria is undoubtedly the most interesting catalytic system. For instance, Cwele

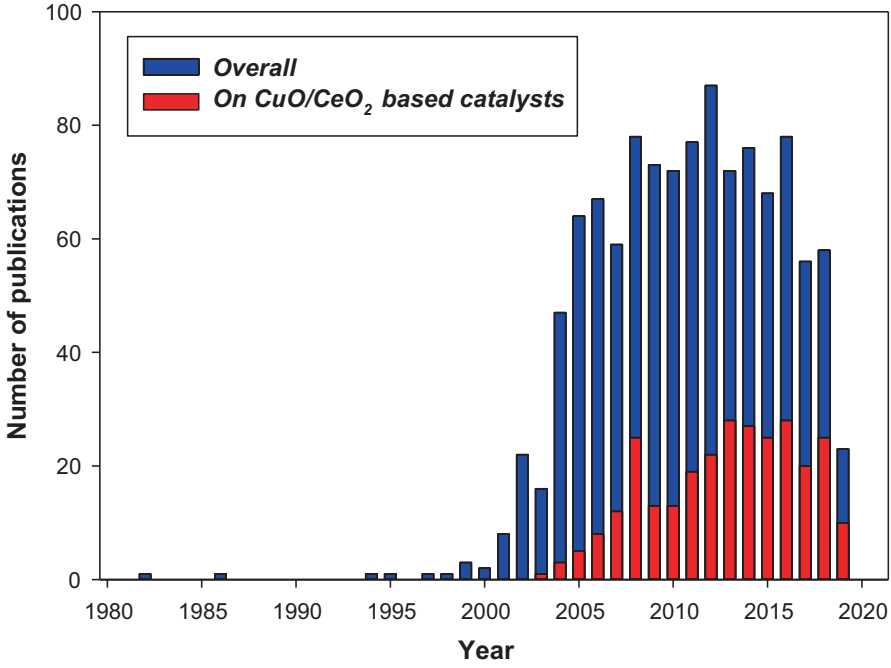

Fig. 3.1 Number of publications related to CO-PROX (blue bars) and focused on CuO/CeO_2 catalysts for CO-PROX (red bars) during the last 40 years (Source: Scopus. Access: May 2019)

et al. [42] and Chagas et al. [43] studied the promoting effect of copper on cobalt substituted ceria and Ni-CeO_2, respectively, and concluded that copper/ceria catalysts, i.e., the system without Co or Ni, showed the best catalytic properties.

As shown in Fig. 3.1, the number of papers devoted to CuO/CeO_2 catalysts for CO-PROX increased rapidly in the mid of 2000s and represents a significant fraction of the overall scientific production related to CO-PROX. It is widely accepted that a key feature, for the good activity of CuO/CeO_2 catalysts, is the strong interactions between copper and ceria resulting in an enhanced reducibility of both oxides [44–46]. It has been evidenced that copper reducibility depends on its dispersion on CeO_2, highly dispersed copper showing the best CO oxidation activity and selectivity [47]. Indeed, copper oxides clusters, not interacting with ceria, are recognized as active centers for the (undesired) H_2 oxidation [48, 49]. According to the above considerations, the nano and subnano structure of CuO/CeO_2 catalysts appears of fundamental interest in order to understand and tune the features affecting catalytic activity and selectivity.

In this chapter, the most interesting results on the effect of nano and subnano structures of CuO/CeO_2 catalysts on the CO-PROX performance are reviewed and critically discussed.

3.2 CuO/CeO_2 Catalysts

As reported above, the interest toward CuO/CeO_2 catalysts has grown during the last few years. Contemporarily, the research was devoted to the comprehension of the nature of the active sites and of the origin of their selectivity. A brief discussion on this topic is necessary before introducing how nanostructure affects the catalytic activity.

To date, a general consensus on the exact nature of the active sites has not been attained. Discussion is open on the oxidation state of active copper [50–55], results supporting both Cu^{2+} and Cu^{+} as active sites for CO adsorption and oxidation. In particular, it is not well established if the active sites for the CO adsorption step are isolated small Cu^{2+} clusters in close contact with CeO_2 [50] or Cu^{+} sites [51]. Moreover, copper active sites are assumed as well as dispersed CuO_x clusters [52], while surface $Cu_yCe_{1-y}O_{2-x}$ has been suggested as active centers by Elias et al. [53] and Arango-Diaz et al. [56].

Nevertheless, some points have been considered accepted and/or more reasonable. First, the key factor for good CO-PROX catalysts is a strong copper-ceria interaction, generally related to a high copper dispersion [57–60]. Moreover, good CO-PROX catalysts require a high (mainly surface and/or subsurface) oxygen mobility related to ceria sites, generally due to the formation of oxygen vacancies [59, 61–63]. It is worth noting that the development of novel in-situ and extra-situ characterization techniques and of more reliable theoretical models allowed a deep understanding of the role of copper-ceria interaction and oxygen vacancies in catalysis and, specifically, in the CO-PROX reaction [64].

In order to improve copper dispersion and to strengthen copper-ceria interaction, several preparation and post-treatment technique were proposed. Preparations included deposition−precipitation [65], incipient wetness impregnation [47, 48, 66, 67], coprecipitation [65, 68–70], sol−gel precipitation [70, 71], solution combustion synthesis [72], urea gelation/coprecipitation [71, 73], “solvent free” synthesis [71]. Examples of post-treatments are reported by Avgouropoulos and coworkers; they showed redispersion of copper species and improved oxygen vacancies under both acid [74] and basic [75] conditions. Du et al. [76] treated the as-calcined CuO/CeO_2 samples with copper loadings as high as 40 at.% with ammonium carbonate aqueous solutions showing that the weakly bonded copper species were removed by the leaching process and replaced by strongly bonded species (active toward CO-PROX) migrating during reduction or reaction condition.

Another key feature related to the strong copper-ceria interaction is the selectivity of the CuO/CeO_2 systems toward CO rather than H_2 oxidation. Several studies reported that the formation of metallic copper enhances H_2 reactivity [47, 69, 77–79], as sketched in Fig. 3.2; thus, over-reduction of copper under reaction conditions leads to the formation of unselective sites. Accordingly, the shift of copper reduction under H_2 at temperature significantly higher than the operation temperature of CO-PROX is beneficial to the catalyst selectivity [80]. Lopez Camara et al. [81] reported that the reduction of ceria particle dimension in an inverse CeO_2/CuO

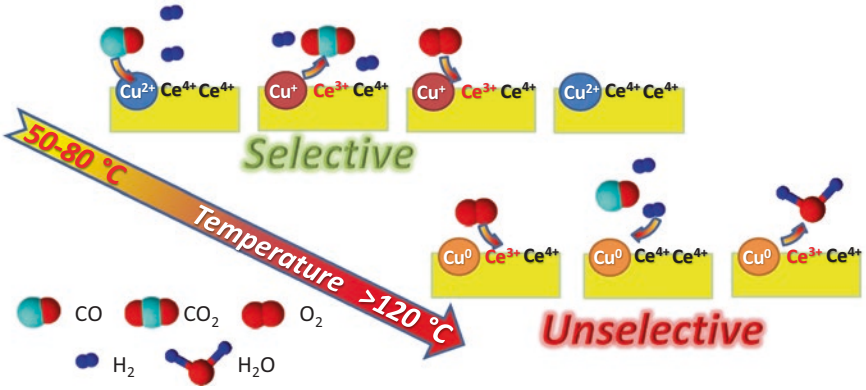

Fig. 3.2 Sketch of the effect of temperature on the copper oxidation state and its influence on the selectivity

catalyst (i.e., a system where ceria is dispersed on copper oxide) delayed copper reduction under H_2 due to a more favored interfacial electron transfer from copper to ceria.

The above considerations suggest that the use of nanoparticles with a high number of copper-ceria contact points can lead to more active and selective CO-PROX catalysts [82]. Indeed, more active structures are formed in the transition to the nanometer range than with the bulk analogs [83]. This is due to change in the unit cell parameters, the mobility of the atoms, the electronic structure, the surface morphology, the reactivity of active centers at the faces, edges, and points of the crystal lattice, etc. The systems formed during the incorporation into nanostructures or inclusion in porous matrices acquire new properties in addition to the individual characteristics of isolated nanosized particles. Such interaction can result in the appearance of additional active centers at the contact points of the nanoparticles. In these systems, a synergic effect seems to be due to the decrease in the energy of electronic transitions in the zones of contact between nanoparticles of different chemical nature [84].

As reported above, this chapter is focused on the relationship between nanostructure and catalytic activity. Results of catalysts characterization, carried out using both conventional and advanced techniques (H_2-TPR, XRD, N_2 physisorption, XPS, and (HR-)TEM), reported in the literature are generally easily comparable. In contrast, catalytic activity is tested under a wide range of experimental conditions differing for CO and/or O_2 concentrations (and thus for CO/O_2 ratio), contact time, and CO_2 and/or H_2O addition (and their concentrations), the only common point generally being the investigated temperature window (i.e., 50–200 °C). The catalytic results are, then, difficult to compare out of a single paper. An attempt was done by López et al. more than 10 years ago [85]; in subsequent years, few works reported a comparison with literature results and generally in a very limited way (for instance, see Di Benedetto et al. [66]). Therefore, in the next sections, catalysts will be not

ranked with respect to their activity and selectivity; the "fil rouge" will be the link among nanostructure, physicochemical feature, and catalytic activity.

3.2.1 How Nanostructure Affects Catalytic Activity

The role of particle dimension has been widely explored for copper-ceria catalysts. Sciré et al. [65] highlighted the effect of ceria nanoparticles in determining the catalytic performance. For instance, Di Benedetto et al. [55] reported the occurrence of CO oxidation at temperature as low as room temperature over a structured catalyst washcoated with CuO/CeO_2 having ceria nanoparticles as the support. The associated transient production of carbon dioxide was related to the high redox properties of the catalyst and, particularly, to the large availability of surface and labile oxygen. The same Authors studied the effect of copper loading on a commercial ceria nanopowder [66]. Outstanding catalytic performances were achieved due to the support nanodimension. In order to observe the effect of copper loading on CO conversion, a contact time as low as 0.027 g s cm^{-3} was necessary. The Authors suggested that on these very active catalysts under certain reaction conditions, the limiting step is not dependent on the copper sites, but more likely on the CO_2 desorption from ceria sites in the neighborhood of copper centers.

A large variety of methods have been used to synthesize ceria-based catalysts with a size as small as possible and, sometimes, with a special morphology, which will be briefly described below.

3.2.1.1 Preparation Techniques

Sciré et al. [65] found that CuCe catalysts prepared by coprecipitation technique have a high surface area and lower ceria particle dimension, which generate higher amounts of defective sites (corners and edges), where oxygen release occurs with a lower energy barrier.

As a consequence, different preparation techniques were proposed in order to produce nanometric catalyst particles.

Maciel et al. [44] obtained CuCe catalysts with particles as small as 5 nm by hydrothermal synthesis with copper content of about 1%, which showed the highest activity with respect to catalysts with higher copper load and larger particles. The same authors [86] prepared both CeO_2 and Cu/CeO_2 samples by hydrothermal synthesis comparing their properties to samples obtained by precipitation with the same composition. The high dispersion of copper in the nanometric support particles prepared by the hydrothermal method led to very good catalytic performance. Moreover, the small crystallites size of ceria (<10 nm) enhanced redox capability and ionic conductivity of CeO_2 due to the higher mobility, primarily of the oxygen ions, important for the CO-PROX mechanism.

Zhang et al. [87] used the urea gelation method to obtain Cu-Ce mixed catalyst with a high surface area and particle dimension of about 10 nm. Furthermore, they obtained mixed CuO and CeO_2 with the same particle size also by mechanical mixing of the two oxides prepared by urea gelation.

Araújo et al. [88] used a microwave assisted hydrothermal synthesis to obtain $Ce_{0.97}Cu_{0.03}O_2$ nanospheres with an average diameter of 20 nm and nanorods with an average diameter of 8 nm and 40 nm in length. Moreover, they observed size reduction of the nanoparticles from 20 to approximately 15 nm with increasing synthesis temperature. Catalysts synthesized at the maximum temperature (160 °C) were those with the best copper dispersion and best CO-PROX performance.

Arango-Diaz et al. [89] used the freeze-drying method to obtain CeO_2 particles with a regular size of 9.5 nm. Copper was successively dispersed. The freeze drying method consisted in a flask freezing of cerium nitrate and Ethylenediaminetetraacetic acid (EDTA) solution using liquid nitrogen to obtain an amorphous precursor which was then calcined.

The same authors used the freeze-drying method to synthesize ceria-zirconia and ceria-alumina supports.

Kosmambetova [84] reported that CeO_2 synthesized from ammonium nitrate precursor was characterized by greater defect structure, lesser occupation of the oxygen positions (increased amount of vacancies), and smaller average size of the crystallites (11 nm) compared with the sample from simple nitrate precursor (13 nm).

One of the effective methods to prepare nanosized catalysts is nanocasting generally using mesoporous silica as a sacrificial template [90]. Advantages of nanocasting method are: (a) uniform and small crystallite size, usually smaller than 10 nm; (b) high surface area and uniform pore size; (c) adjustable structure; and (d) crystalline framework, with domain sizes that do not increase with increase in synthesis temperature [68]. Gu et al. [68] synthesized ordered mesoporous Cu–Ce–O catalysts with different copper contents (5–70 mol%) using mesoporous silica KIT-6 as a hard template in one-step nanocasting method with a surface area as high as 159 $m^2\ g^{-1}$. The catalysts nanocasted in one step show better performance than the ones prepared by a two-step impregnation method.

A more unusual technique was also proposed [91, 92] using the highly ordered HKUST-1 with a microporous structure and a long copper–copper dimer distance (well separated by the 1,3,5-benzene-tricarboxylate (BTC) ligand with a distance of 0.8 nm) as the hard template to disperse cerium ions, which can be uniformly adsorbed into the channel of $Cu_3(BTC)_2$ (Fig. 3.3). After removing the organic ligand by thermal treatment, copper and ceria remain well distributed. The use of a nanoporous host provided 10–11 nm CuCe crystals after thermal treatment at 500–600 °C with very high CO-PROX performance.

Li et al. [93] used a special technique to produce CeO_2 nanoparticles (5 nm average size) with highly dispersed copper: the melt infiltration method into silica hollow nanospheres starting from cerium and copper nitrate precursors. They reported that this method allows an effective dispersion of precursor salts in the pores of the silica hollow nanospheres providing the maximum activity for a Cu/Ce ratio 1/8.

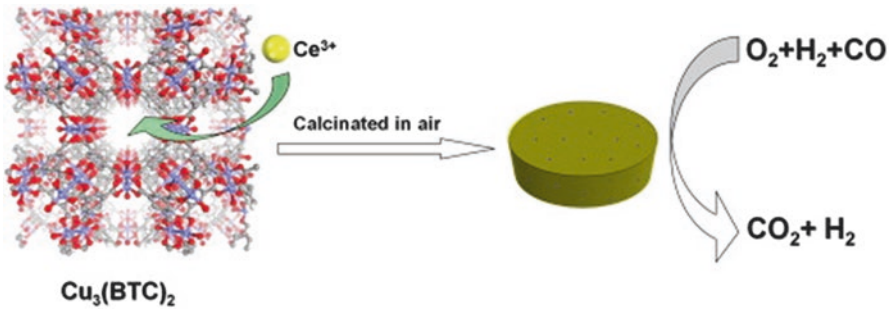

Fig. 3.3 CuO/CeO_2 catalyst prepared by MOF precursor for CO-PROX (From Zhang et el. [91] Copyright © 2012 Elsevier B.V. Reproduced with permission)

Tang et al. [94] proposed a facile solid state impregnation method to prepare $CuO\text{-}CeO_2$/SBA-15 catalysts. Both copper and ceria were well dispersed on SBA-15, and the CO-PROX activity was greatly enhanced, which could be attributed to the distinct reduction of ceria size.

Gong et al. [95] used the surfactant template method to produce both CeO_2, MnO_x and $CeO_2\text{-}MnO_x$ with nanometric size (<8 nm), which was preserved also after dispersion of CuO by wet impregnation. The same authors [95] obtained similar dimension of $CeO_2\text{-}MnO_x$ mixed oxides using both deposition-precipitation and surfactant template methods. The same effect was obtained by Zeng et al. [96] always on $MnO_x\text{-}CeO_2$ synthesized by the hydrothermal method but for the preparation of inverse catalysts. The $MnO_x\text{-}CeO_2$ particles on CuO have maximum 7 nm dimension.

Liu et al. [97] prepared the $CuO–CeO_2$ catalyst by coprecipitation and ethanol washing obtaining nanosized samples with a high surface area. They also found lattice defects over the surface of $CuO–CeO_2$, which are beneficial to enhance catalytic performance.

Chung and Yeh [98] prepared $CuO–CeO_2$ nanocomposites by coprecipitation of nitrates at changing pH values. They found that precipitation at high pH led to a high concentration of CeO_2 nucleation and significant number of Cu sites at interface between CuO and CeO_2. They also demonstrated that the samples obtained at high pH values exhibited very high CO conversion and selectivity.

Marban et al. [99] synthesized CuO_x/CeO_2 nanocatalysts using the silica aquagel coprecipitation (SACOP). They found very good performance in terms of both catalytic activity and selectivity. However, they also found catalyst deactivation. From their analysis it turns out that the reason for the catalyst deactivation is related to the formation of surface carbonates and to the aggregation of dispersed Cu^{2+} in CuO clusters.

Conversely, Sedmak et al. [100] showed that the nanostructured $Cu_{0.1}Ce_{0.9}O_{2-y}$ catalyst prepared by a sol–gel method exhibits very stable operation also under severe reducing conditions.

Xu et al. [101] prepared Cu-doped cerium oxide nanofiber catalyst via electrospinning. They obtained samples with high surface areas and a special fiber-like nanostructure with highly dispersed and active Cu^{2+} ions.

As shown in Fig. 3.4, nanofibers present length of about 50 μm and a diameter of about 200 nm. The TEM images also show the presence of a large quantity of nanofibers with an average diameter of about 8.5 nm.

A simple way to prepare nanocomposite catalysts was suggested by Borchers et al. [102]. They found that a 60 min ball milling procedure allowed to generate CuO/CeO_2 nanoparticles agglomerated into larger aggregates (Fig. 3.5). The milled catalysts showed improved catalytic activity due to a better copper dispersion and larger Cu^+ fraction.

In Table 3.1 the performances and the average nanometric size of most of the best catalysts discussed above are reported.

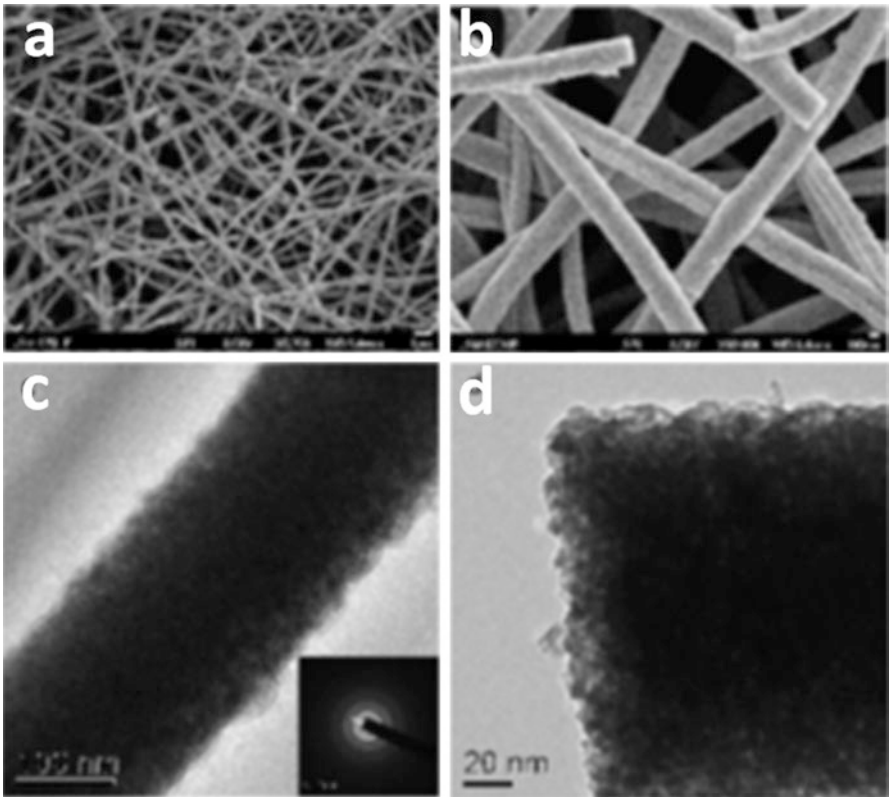

Fig. 3.4 SEM images of $Cu_{0.1}Ce_{0.9}O_{2-x}$ nanofibers (NFs) at low magnification (**a**) and high magnification (**b**); TEM images of a single $Cu_{0.1}Ce_{0.9}O_{2-x}$ nanofiber at low magnification (**c**) and high magnification (**d**) (From Xu et al. [101] Copyright © 2011 Elsevier B.V. Reproduced with permission)

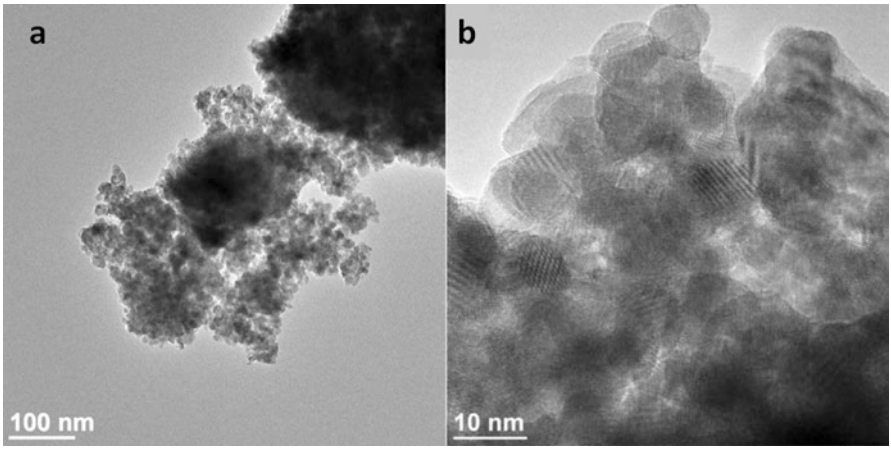

Fig. 3.5 (**a**) TEM micrograph of CuO-CeO_2 powder milled for 60 min; (**b**) enlargement showing dimension and shape of agglomerated nanoparticles (From Borchers et al. [102] Copyright © 2016 Elsevier B.V. Reproduced with permission)

Table 3.1 Performance of catalysts prepared by different preparation techniques: average particle size (*d*, nm), best CO conversion (*x*, %) and corresponding selectivity to CO_2 (*s*, %), temperature (*T*, °C), and contact time (*W*/*F*, g s cm^{-3})

Preparation techniques	*d*	*x*; *s*[a]	*T*[b]; *W*/*F*	References
Coprecipitation	6	95; 62	150; 0.038	[65]
Wet impregnation	<20	100; 100	110; 0.027	[55]
Hydrothermal synthesis	5–8	100; 100	110; n. a.	[44]
Urea gelation	11	n.a.; n.a.	60; n. a.	[87]
MW assisted hydrothermal synthesis	20	92; n. a.	150; n.a.	[88]
freeze-drying method	12	100; 97	90; 0.18	[89]
Nanocasting with mesoporous silica	8–9 (crystal)	100; 100	40; 0.097	[90]
Nanocasting with mesoporous silica	23 (crystal)	99; 50	170; 0.06	[68]
Thermal treat. of $Cu_3(BTC)_2$ precursor	11 (crystal)	100; 100	90; 0.2	[91]
Melt infiltration	5	90; 60	175; 0.0045	[93]
Surfactant template method	5 (crystal)	100; 50	140; 0.06	[95]
Ethanol washing	10 (crystal)	100; 95	120; 0.03	[97]
Coprecipitation at various pH	6	100; 100	120; 0.006	[98]
Silica aquagel coprecipitation (SACOP)	2–3 (crystal)	95; 68	208; 0.06	[99]
Electrospinning	8.5 (crystal)	100; 92	120; 0.3	[101]

n.a. not available (catalyst mass or flow rate not reported)

[a]Values of conversion and selectivity can be indicative in some cases because extracted from graphs. CO conversion reported is the best conversion obtained with the best performing catalyst. The value of selectivity is that corresponding to the best conversion

[b]Temperature corresponding to the best conversion

3.2.1.2 Particle Morphology

As reported by Trovarelli and Llorca [83], not only the dimension but also the shape of CeO_2 nanoparticles can significantly affect the metal-support interaction, thus providing enhancement of activity and selectivity. Thus, at the beginning of the last decade, in addition to the nanometric dimension the effect of ceria morphology was also investigated producing CeO_2 particles as stars, cubes, rods, etc.

Han et al. [103] synthesized ceria nanocrystals in different shapes: octahedra, rods and cubes with 10–20 nm dimension. They found that copper was deposited at higher concentration on octahedra but it better migrates from bulk crystal to the surface for rods. This determined a different CO-PROX activity at low and high temperature, rods working better at high temperature and cubes at lower temperature. On the other hand, Monte et al. [104] found that ceria nanocubes were the most selective due to the greater exposure of {001} facets, coordinatively more unsaturated, promoting a stronger interaction with copper.

Gamarra et al. [105] investigated the catalysts morphologies and obtained both CeO_2 support and Cu/CeO_2 catalysts with particles dimension as low as 7 nm as nanospheres (Fig. 3.6). These catalysts showed a better CO-PROX activity at low temperature with respect to nanocubes or nanorods with a larger dimension and lower surface area although they also found an effect of crystalline faces exposure on selectivity.

The effect of the phase exposure was also reported by Guo and Zhou [106]. They compared CuO/CeO_2 catalysts synthesized by the impregnation method on differently shaped ceria (rod, cube, plate and polyhedral), showing that CuO/CeO_2-rod and CuO/CeO_2-polyhedra exhibit a higher low-temperature catalytic oxidation activity coupled with a broader operating temperature window, while CuO/CeO_2-cube showed the worst performance. The reason was found in the improved dispersion of copper with a stronger interaction on the ceria rods and polyhedra.

Accordingly, Xie et al. [107] demonstrated that copper-ceria interaction is favored onto {111} and {002} ceria planes; so, nanospheres and nanospindles are

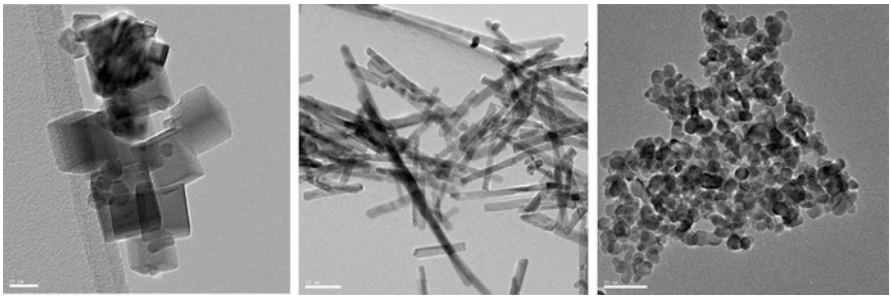

Fig. 3.6 TEM images of the different CeO_2 supports: CeO_2-nanocubes (left), CeO_2-nanorods (middle) and CeO_2-nanospheres (right). The horizontal scale bar shown corresponds to 50 nm except for CeO_2-NC for which it represents 20 nm (From Gamarra et al. [105] Copyright © 2013 Elsevier B.V. Reproduced with permission))

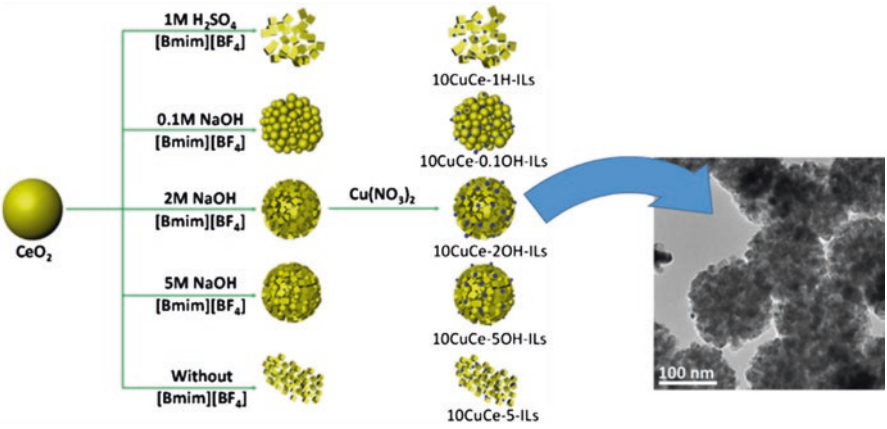

Fig. 3.7 Schematic illustration of the synthetic procedures of Cu_xO/CeO_2 nanocube catalysts and TEM image of the sample providing the best catalytic activity. Adapted from Gong et al. [109] (Copyright © 2017 Elsevier B.V. Reproduced with permission)

the preferred nanoshaped supports. Onto these supports in the presence of copper, the oxygen vacancies fraction is increased, thus improving the oxygen transfer from copper to ceria, according to the following equation.

$$Cu^{2+} + Ce^{3+} \rightarrow Cu^{+} + Ce^{4+} \tag{3.4}$$

Kou et al. [108] prepared CuO/CeO_2 nanowires starting from $Al_{90}Cu_{2.5}Ce_{7.5}$ (at%, nominal concentration) alloy ribbons by a de-alloying procedure in 5 M NaOH aqueous solution. The so-prepared catalysts preferentially expose the {110} ceria plane and showed good activity toward CO-PROX due to good copper dispersion and oxygen mobility.

Gong et al. [109] prepared ceria nanocubes by acid or basic treatment of nanospheres with an ionic liquid (IL) of 1-butyl-3-methylimidazolium tetrafluoroborate ([Bmim][BF_4]) under hydrothermal condition and used them as support for CuO/CeO_2 catalysts (Fig. 3.7). The best results were obtained with a 2 M NaOH solution, providing the best copper-ceria interaction. Figure 3.7 shows a TEM image of this catalyst.

In Table 3.2 the performances and the average nanometric size of most of the best catalysts discussed above are reported.

3.2.1.3 Inverse CuO/CeO_2 Catalysts

In the same years also inverse catalysts were proposed. In these catalysts CeO_2, generally as nanoparticles, is deposited on CuO in order to enhance the number of contact points between the two oxides where active sites are supposed to be located. In 2010 Martinez-Arias and coworkers [110] first reported the inverse CuO/CeO_2

Table 3.2 Performance of catalysts characterized by different shapes: average particle size (*d*, nm), best CO conversion (*x*, %) and corresponding selectivity to CO_2 (*s*, %), temperature (*T*, °C), and contact time (*W*/*F*, g s cm^{-3})

Shape	*d*	*x*; *s*[a]	*T*[b]; *W*/*F*	References
Octahedra	15.3	95; 50	140; 0.1	[103]
Rods	n.a.	85; 70	170; 0.12 (in situ Drift)	[104]
Cubes	46	>99;70	170; 0.12	[105]
Polyhedra	5–10	>99; 100	85; 0.06	[106]
Spheres	180	100; 100	80; 0.09	[107]
Wires	20	100; 93	95; 0.45	[108]
Cubes	14.1	100; 70	150; 0.06	[109]

n.a. not available

[a]Values of conversion and selectivity can be indicative in some cases because extracted from graphs. CO conversion reported is the best conversion obtained with the best performing catalyst. The value of selectivity is that corresponding to the best conversion

[b]Temperature corresponding to the best conversion

catalyst for preferential CO oxidation. They showed that the amount and properties of copper-ceria interfacial sites in the inverse system keep a high level of CO oxidation activity due to the structure sensitivity of these catalysts.

The inverse CeO_2/CuO catalysts show a wider CO conversion window and higher CO_2 selectivity in comparison with the classical CuO/CeO_2 catalyst [111]. A synergistic effect occurs at the interface of the CeO_2-CuO catalyst and the particle sizes of CuO and CeO_2 directly determine the perimeter and area of this contact interface.

Different preparation techniques were proposed to prepare the inverse catalysts. Zeng et al. [111] prepared inverse catalysts using the solvothermal method to obtain the CuO precursor with cotton-ball-like morphology and CeO_2/CuO catalysts with a high BET surface area. The authors confirmed that the CO-PROX reaction takes place at the interface of the nanometric (<10 nm) CeO_2 particles and CuO.

Zeng et al. [112] compared direct and inverse copper cerium catalysts both prepared by the hydrothermal method. TEM analyses indicated that the inverse CeO_2/CuO catalyst has CeO_2 crystallites with a dimension of about 3–8 nm gathered into many small islands dispersed on the bulk CuO with 20–50 nm size. The traditional CuO/CeO_2 catalyst shows better activity at lower temperature and the inverse CeO_2/CuO catalyst present higher CO_2 selectivity when the CO conversion reaches 100% since it can still supply sufficient CuO for CO oxidation $T < 200$ °C. In the inverse sample the bulk CuO can chemisorb CO and H_2 at the suitable temperature and the small islands of CeO_2 can provide oxygen for CO and H_2 oxidation. This confirms that the reaction occurs at the contact interface of the CeO_2 islands and bulk CuO.

Zeng et al. [113] also proposed CeO_2/CuO catalysts prepared by hydrothermal method using Na_2CO_3 as precipitant with different Cu/Ce ratio. They obtained CeO_2 particles of about 10 nm and CuO particles with about 20 nm dimension. The CeO_2 particles self-assemble into the rod-like structures during the hydrothermal procedure and the rods of CeO_2 become shorter with the decrease of Ce/Cu molar ratio.

Furthermore, copper cations enter into the lattice of CeO_2 and the highly dispersed CuO are favorable for CO oxidation at lower temperature.

The same authors [114] used different precipitants (urea, NaOH, tetramethylammonium hydroxide) for a reverse microemulsion impregnation method to obtain inverse catalysts with an average particle size of 5 nm. They reported that the catalytic performance was closely associated to the extent of the contact interface between CeO_2 and CuO depending on the crystal sizes of CeO_2 and CuO. In a subsequent work [115] they found that CeO_2/CuO catalyst starting from urea precipitant was that with the smallest CuO crystallites. The particle-like structure consists of bulk CuO and filamentous and bowl-like structures of 5 nm CeO_2 crystallites.

Zeng et al. [116] also proposed CeO_2 nanoparticles supported on CuO with sphere-flower and petal-like morphologies. The particle size of CuO support was about 20 nm whilst that of CeO_2 dispersed particles was about 5 nm. They supposed a semi-spherical shape of CeO_2 particles because they observed an increase of TOF with increasing CeO_2 size. In fact, this maximizes the copper-cerium contact confirming that active sites are located at cerium-copper interface.

The same authors prepared rod-like CeO_2 particles with an average size of 10 nm dispersed on CuO by hydrothermal method with different Cu/Ce molar ratio. The smaller CeO_2 easily entered into the crystal lattice of CuO. Moreover, the rod-like CeO_2 exposed more {111} planes, representing those with the highest oxygen storage and transportation capacity. The contact interface of highly dispersed ceria and bulk CuO was more favorable to CO oxidation than to H_2 oxidation thus providing the best catalytic performance.

Zeng et al. [117] used the surfactant template method to synthesize both CuO/CeO_2 and inverse CeO_2/CuO catalysts to investigate the active sites that they supposed located at the contact interface between the two oxides. They obtained both CuO and CeO_2 with nanometric dimension.

The hydrothermal in combination with impregnation method was used to prepare the CeO_2/CuO catalysts with spherical structure [118]. The microspheres of CuO (20–25 nm) consist of the sheet-like CuO and the way of arrangement results in the formation of a shell structure. The core in the middle of shell structure was composed of the nanosized CuO particles. CeO_2 particles are supported on the surface of the CuO microspheres or embedded in the pores of sheet-like CuO and their size was 6–7 nm.

Catalysts in inverse configuration (CeO_2/CuO) were also proposed by López Cámara [119] with CeO_2 nanoparticles (4.9 nm) deposited on larger (12–20 nm) CuO nanoparticles. They also reported that the addition of ZnO nanoclusters further reduced both CeO_2 (3.9 nm) and CuO particle dimension and that resulted most favorable to the CO-PROX catalytic properties. On the basis of their results, they suggested that the crystal size of CeO_2 was a relevant parameter to tune CO-PROX characteristics of this type of inverse CeO_2/CuO catalysts.

Chen et al. [120] proposed a multistep process for synthesizing CeO_2 nanoparticles on Cu with a large concentration of oxygen vacancies using urea as the additive and NaOH as the precipitation agent. The HR-TEM analysis confirmed the presence on Cu surface of pillar-shaped CeO_2 nanoparticles with a diameter less than 10 nm

Table 3.3 Performance of different inverse CeO_2/CuO catalysts: best CO conversion (x, %) and corresponding selectivity to CO_2 (s, %), temperature (T, °C), and contact time (W/F, g s cm^{-3})

Catalyst	x; s[a]	T[b]; W/F	References
CeCu	>99; 100	90; 0.06	[110]
CeCu	100; 75	110; 0.09	[111]
CeCu	>99; 100	100; 0.09	[112]
CeCu	>99; 100	140; 0.09	[114]
CeCu	100; 80	160; 0.09	[115]
CeCu	100; 100	150; 0.09	[116]
CeCu	100; 100	100; 0.09	[117]
CeCu	100; 90	130; 0.09	[118]
CeCu-Zn	100; 100	150; 0.06	[81]
CeCu	100; 93	120; 0.2	[123]
CeCu	90; 60	160; 0.075	[121]
CuCe	100; 88	120; 0.09	[122]

[a]Values of conversion and selectivity can be indicative in some cases because extracted from graphs. CO conversion reported is the best conversion obtained with the best performing catalyst. The value of selectivity is that corresponding to the best conversion
[b]Temperature corresponding to the best conversion

with a fluorite-type structure. Oxygen vacancies were generated as a consequence of electron donation from metal copper atoms to the CeO_2 acceptor and the subsequent reverse spillover of oxygen induced by electron transfer in a well-controlled nanoheterojunction. The anchored oxygen vacancies play a bridging role in electron capture or transfer and drive oxygen molecules into active oxygen species to interact with the CO molecules adsorbed at interfaces, thus leading to an excellent preferential CO oxidation performance.

Gu et al. [121] prepared ceria nanorods and investigated the role of the copper content. The best catalyst was characterized by a Cu/Ce ratio equal to about 2.5. With respect to the other samples in the best catalyst, the Cu^+ and the Ce^{3+} fractions were enhanced.

Xie et al. [122] prepared inverse CeO_2/CuO catalysts by using star-shaped Cu_2O particles. Ceria was detected as nanoparticles dispersed onto the Cu_2O surface. Despite the starting copper oxidation state was one, the Authors related the catalytic activity to the coexistence of Cu^{2+} and Cu^+; in particular, they linked the redox copper cycle to the redox cerium cycle.

In Table 3.3, the performances and the average nanometric size of most of the best catalysts discussed above are reported.

3.2.1.4 CuO/CeO_2 on Carbon

In order to get strong copper-ceria interaction and a very high surface area, CuO/CeO_2 catalysts were supported onto carbon nanotubes and similar structures. Zeng et al. [124] supported CuO/CeO_2 onto multiwall carbon nanotubes (MWCNTs). The

catalyst with 20 wt% CuO and equimolar amounts of copper and cerium showed the best catalytic activity; the sample was characterized by a large specific surface area (about 150 $m^2\ g^{-1}$). The pore diameter of carbon tubes was about 20 nm before active phase deposition, decreasing down to 12 nm on the catalyzed systems, while ceria particles showed wire shape with almost 7 nm characteristic dimension. Results showed a relation between copper interaction with ceria, Ce^{3+} fraction (i.e. oxygen vacancies) and catalytic activity, thus confirming other results on this topic. On the other hand, the use of multiwall carbon nanotubes with a high surface area seemed to weaken the poisoning effect of H_2O and CO_2.

Similarly, Gao et al. [125] supported CuO/CeO_2 catalysts on MWCNTs with different Cu/Ce ratios and compared with Cu/CeO_2 supported onto activated carbon, γ-alumina and silica. Best performance was measured on the catalyst showing an equimolar ratio between copper and cerium supported onto MWCNTs. The Authors related the catalytic properties to a unique interaction between the active phase and the support, providing also the highest Ce^{3+} fraction.

Dongil et al. [126] supported copper-ceria catalysts onto carbon nanotubes (CNT) and graphene oxide (GO) and investigated the effect of K addition. Figure 3.8 shows TEM images of the investigated samples. Catalysts deposited onto CNTs were more active than those supported onto GO due to a better active phase dispersion. Moreover, K doping ($K \leq 1.0$ wt.%) resulted in an improved ceria dispersion and stronger copper-ceria interaction, thus improving catalytic performance toward CO-PROX.

Zeng and coworkers used reduced graphene oxide (RGO) as CuO/CeO_2 support in combination with MWCNTs [127] or alone [128]. In the absence of MWCNTs [128], the best catalyst was characterized by a Cu/Ce ratio equal to 1. Good copper and cerium dispersions were detected, suggesting good interaction; moreover, significant fractions of Cu^+ and Ce^{3+} were measured and related to the good catalytic activity. In addition, the sample showed improved resistance to the inhibiting effect of carbon dioxide and water vapor, probably due to the formation of hydroxyl groups by dissociative adsorption of H_2O on the surface of reduced graphene oxide. MWCNTs added to this catalyst [127] acted as spacer between RGO sheets both improving copper oxide and ceria dispersion and enhancing the concentration of oxygen vacancies. So, the ternary nanocomposite showed better performance toward CO-PROX reaction.

Zhang et al. [129] also prepared CuO/CeO_2 (Cu/Ce = 1) catalysts supported on reduced graphene oxide according to the procedure sketched in the Fig. 3.9. It is nothing that the active phase is dispersed as nanoparticles onto the support; additionally, the Authors suggested that CuO/CeO_2 particles were wrapped up in RGO layers with close interfacial interaction, thus providing optimal spatial condition for charge transport between RGO layers and CuO/CeO_2.

Shi et al. [130] supported CuO/CeO_2 with different Cu/Ce ratios onto commercial MWCNT by a special ultrasound-aided impregnation. The sample with a Cu/Ce ratio equal to 0.67 showed the best catalytic properties due to an enhanced copper reducibility and a good dispersion of CuO and CeO_2 particles. They also accounted for a higher fraction of oxygen vacancies.

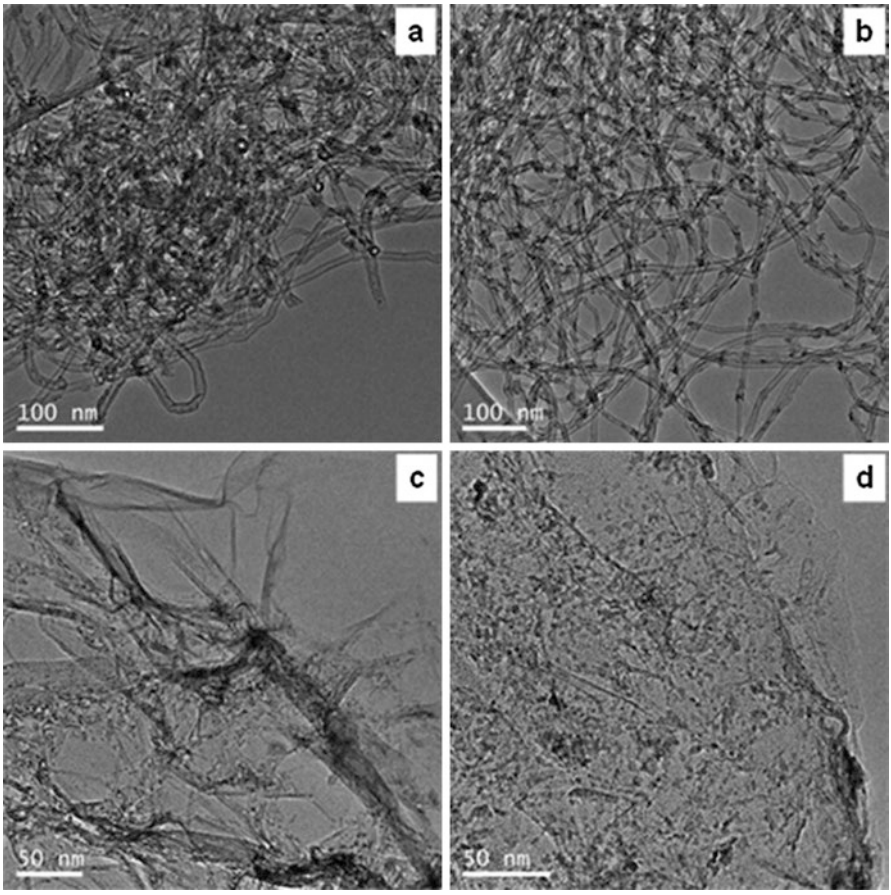

Fig. 3.8 TEM images of Cu/CeO_2 catalysts supported onto carbon nanotubes (**a**, **b**) and onto graphene oxide (**c**, **d**). Samples in figures **b** and **d** are doped with potassium (From Dongil et al. [126] Copyright © 2016 Royal Society of Chemistry Reproduced with permission)

In Table 3.4, the performances and the average nanometric size of most of the best catalysts discussed above are reported.

3.2.2 How Doping Affects Nano (and Subnano) Features

Improving catalytic activity and selectivity means improving copper dispersion and Cu-Ce interactions, thus reducing the typical dimension of the copper aggregates, i.e., the active sites. To this end, addition of other elements to Cu-Ce catalysts was used to improve catalytic properties.

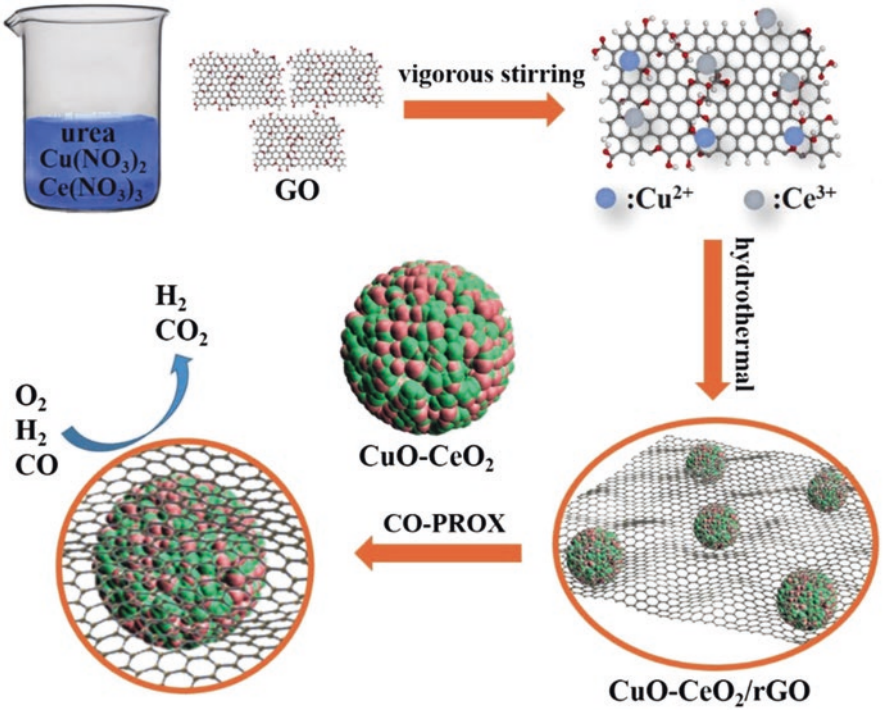

Fig. 3.9 Sketch of the preparation of RGO/CuO/CeO_2 catalysts (From Zhang et al. [129] Copyright © 2018 Springer Nature Reproduced with permission)

Table 3.4 Performance of CuCe catalysts supported onto different carbon-based supports: average particle size (*d*, nm), best CO conversion (*x*, %) and corresponding selectivity to CO_2 (*s*, %), temperature (*T*, °C), and contact time (*W*/*F*, g s cm^{-3})

Carbon support	*d*	*x*; *s*[a]	*T*[b]; *W*/*F*	References
MWCNT	7.0	100; 100	110; 0.09	[124]
MWCNT	4.3	100; 100	130; 0.03	[125]
CNT (+ K-doping)	4.2	100; 70	175; 0.03	[126]
RGO/MWCNT	2.8	100; 55	120; 0.09	[127]
RGO	3.2	95; 70	140; 0.09	[128]
RGO	100–220	100; 90	120; 0.06	[129]
CNT	n.a.	100; 100	120; 0.09	[130]

n.a. not available

[a]Values of conversion and selectivity can be indicative in some cases because extracted from graphs. CO conversion reported is the best conversion obtained with the best performing catalyst. The value of selectivity is that corresponding to the best conversion

[b]Temperature corresponding to the best conversion

Zr has been generally added to CeO_2 to improve performance, as occurring in TWCs. However, often different and, in some cases, opposite results are found in the literature. A positive effect was reported by Martinez-Arias et al. [131] and Reddy et al. [132]. On the contrary, Caputo et al. [133] and Ayastuy et al. [134] reported that adding Zr to the support decreases both activity and selectivity with respect to CuO/CeO_2 catalyst which outperforms with respect to $CuO/Ce_xZr_{1-x}O_2$ and is much better than CuO/ZrO_2. Wang et al. [135] proposed highly performing $CuO_x/Ce_{0.8}Zr_{0.2}O_2$ catalysts prepared by a facile and rapid route (urea grind combustion method) with a very small dimension (about 10 nm). The use of this preparation technique avoids the formation of bulk unselective CuO and also provides a good tolerance to CO_2 and H_2O.

Guo et al. [136] modified the redox properties of CuO supported onto CeO_2 nanorods by doping the ceria rods with Mn, Ti, Zr, and Ni. Mn and Ti addition provided higher activity, selectivity and resistance to the inhibition effect of CO_2 and H_2O, while Zr showed a marginal effect and Ni decreased the catalytic performance. Both Mn and Ti promoted the formation of surface defects and oxygen vacancies and incorporation of isolated copper. However, while Mn improved low temperature oxygen mobility due to its surface existence with multiple valence states, Ti promoted the formation of a perovskite-like structure enhancing copper dispersion and interaction with the support. An evident promoting effect of low Mn amounts (Mn/(Mn + Ce) = 0.05) was reported by Jin et al. too [137]. The main reason was attributed to the formation of Ce-Cu-Mn-O ternary solid solution, causing the formation of more oxygen vacancies, an improved reducibility and an increased amount of surface oxygen species. Further Mn addition decreased the catalytic performance and lowered the related physicochemical features.

Cecilia et al. [138] compared CuO/CeO_2 catalysts doped with Zr, La, Tb, and Pr to an undoped reference sample. Under "ideal" reaction conditions (i.e., in the absence of CO_2 and H_2O) the doped samples showed higher catalytic activity than the undoped one (except the La-doped sample), Zr-doped catalyst showing the best performance. These results suggested a relationship between the dopant charge and the catalytic activity, 4+ cations being thus preferable. However, under "real" reaction conditions (i.e., in the presence of CO_2 and H_2O) no significant difference among the sample was detected.

Also, the Nb addition was ineffective to improve the catalytic behavior of CuO/CeO_2 catalysts [139]. As a matter of fact, niobia did not modify the redox properties of the catalyst, i.e., it did not change the copper-ceria interaction, but it introduced acid sites useless for CO-PROX reaction.

As reported in the Sect. 3.1, Pt and Au based catalysts are very active toward CO-PROX. Accordingly, several efforts have been done in order to combine the good properties of CuO/CeO_2-based catalysts with those of Pt and Au.

Kugai et al. [140] reported that nanosized CuO particles or clusters interact with CeO_2 surface to exhibit synergistic effect in reducibility at the interfacial area. CO adsorbs on copper sites and oxygen is supplied from CeO_2 through the interface. Although CuO/CeO_2 shows high selectivity, it has drawback of slow kinetics at low CO concentration which makes noble metal still necessary for deep CO removal

from H_2 stream. For this reason, they developed supported PtCu alloy nanoparticles (3–4 nm) synthesized by a unique radiation-induced synthesis process supported on CeO_2. This radiolytic process is described as a simple method to obtain nanoparticles with well-controlled structure and size through irradiating the aqueous ions of metal sources with no need for post-treatment by heat or other chemicals.

Cu-Pt alloy nanoparticles with a slightly higher dimension (4–5 nm) were deposited on CeO_2 or γ-Fe_2O_3 by the same authors by electron beam irradiation method [141, 142]. They also found that Pt-Cu with CeO_2 of small crystallite size had highest activity and selectivity in CO-PROX, preserved also when water was added in the mixture. The high oxygen transport capacity was attributed to small CeO_2 crystallite size (average size 24 nm).

In the work of Lang et al. [143] copper and platinum were loaded simultaneously on the ceria-coated alumina sponge by means of supercritical fluid reactive deposition (SFRD), which consists in adsorption and reduction of metal-organic complexes dissolved in supercritical CO_2. Nanosized copper inside and in close contact with the ceria layer provided a good reducibility and thus high activity of the catalyst.

About Au-doped CuO/CeO_2 catalysts, the formation of Au-Cu alloys has been reported [144–148]. In particular, alloys with nanometric dimension (5–10 nm) with preset stoichiometry dispersed on different support (SiO_2, CeO_2, γ-Al_2O_3) were prepared by Potemkin et al. [147] starting from $[Au(en)_2](NO_3)_3$ and $(NH_4)_2[Cu(C_2O_4)_2]\cdot 2H_2O$ complex compounds. These catalysts showed a higher selectivity in the realistic hydrogen-rich mixture containing CO_2 and H_2. Interestingly, Papavasiliou [148] reported decoration of CuO nanoparticles with gold (metallic and cationic) clusters; the presence of these species was related to the improved CO-PROX performance.

The promoting effect of iron addition to CeO_2 or CuO/CeO_2 mixed oxide has been studied in several papers [61, 80, 149–154]. Firsova et al. [149] reported a positive effect of iron addition due to the role of iron in the redox cycles, while Bao et al. [153] suggested that the improved catalytic activity of a Fe_2O_3–CeO_2 composite was related to the density of surface oxygen vacancies promoted by iron addition. Results reported in further papers confirmed that iron addition improved the catalytic properties by modifying the nanostructure of the catalysts. In particular, improved copper dispersion (and thus copper-ceria interaction) [80] and the generation of more oxygen vacancies, enhancing the Cu-Ce interaction, trapping the gas-phase oxygen, and promoting the mobility of subsurface lattice oxygen, [61] were claimed to explain the Fe-promoting effect. Recently, Dasireddy et al. [155] prepared bimetallic Cu-Fe/CeO_2 and Cu-Co samples supported onto carbon nanotubes (CNT) and compared their features and performance to those of monometallic ones. The Authors detected the formation of a $CuFe_2O_4$ phase enhancing the copper dispersion. From the catalytic point of view, the Fe-promoted sample showed a significant resistance to the inhibiting effect of CO_2 and H_2O. In particular, CO_2 acted as inhibitor, while H_2O as promoter. The latter effect was probably due to the formation of hydroxyl group on the surface, boosting the catalytic activity, in agreement with Bueno-Lopez and coworkers [54]. In contrast, on a Fe-promoted CuO/CeO_2

Table 3.5 Performance of CuCe catalysts doped with different elements: average particle size (*d*, nm), best CO conversion (*x*, %) and corresponding selectivity to CO_2 (*s*, %), temperature (*T*, °C), and contact time (*W*/*F*, g s cm^{-3})

Dopant	*d*	*x*; *s*[a]	*T*[b]; *W*/*F*	References
Zr (Ce/Zr = 4)	10	100; 100	120; 0.15	[135]
Mn (Mn/(Mn + Ce) = 0.05)	8	100; 100	100; 0.06	[136]
Pt (Cu/Pt = 9)	4 (PtCu particles)	100; 30	90; 0.12	[140]
Au (0.15 wt.%)	5–15	100; 90	120; 0.144	[148]
Fe (5 wt%)	n.a.	100; 75	140; 0.054	[80]
K (K/Cu = 0.68)	4.2	100; 75	175; 0.03	[158]

n.a. not available

[a]Values of conversion and selectivity can be indicative in some cases because extracted from graphs. CO conversion reported is the best conversion obtained with the best performing catalyst. The value of selectivity is that corresponding to the best conversion

[b]Temperature corresponding to the best conversion

catalyst, both CO_2 and H_2O lowered the catalytic performance [156]. The Authors reported that the CO_2 showed the most inhibiting effect, even higher than $CO_2 + H_2O$, while H_2O addition slightly decreased the catalytic activity. Therefore, iron-promoted catalysts seem to be less sensitive to H_2O addition. However, the promoting effect of H_2O detected by Dasireddy et al. [155] could also be due to the CNT support.

Doping with potassium was demonstrated to be effective to enhance the catalytic properties of CuO/CeO_2 catalysts, especially in terms of resistance to the inhibiting effect of CO_2 and H_2O [157]. More recently, Dongil et al. [158] investigated the whole group of alkalis (Li, Na, K, Cs), added to CuO/CeO_2 samples supported onto carbon nanotubes, thus expanding their previous study on K-doped catalysts [126]. The results suggested a significant role of the nature of the alkali element on the dispersion of ceria and the Cu-ceria interaction. This was also due to the formation of CeO_2 particles with small crystal size (4–6 nm) in the presence of alkalis (except Cs). These features were related to the improved catalytic performance of K-, Li-, and Na-doped samples, respectively. In contrast, Cs showed a detrimental effect on the CO-PROX activity.

In Table 3.5, the performances and the average nanometric size of most of the best catalysts discussed above are reported.

3.3 Conclusions and Outlooks

The preferential oxidation of carbon monoxide poses both fundamental and applicative issues. Research was, thus, devoted both to investigate the relationship between physicochemical features and catalytic properties and to engineer effective catalysts. From this point of view, copper-ceria catalysts are very intriguing. From the beginning of their exploration, it was clear that the copper-ceria interaction and,

thus, the copper dispersion play a fundamental role, pushing the research at nanoscale levels.

Reduction of ceria size to nanoparticles showed a positive effect on the catalytic properties of CuO/CeO_2 systems and several preparation methods were proposed for this purpose. The nanodimensions improve both Cu dispersion and oxygen mobility and prevent, at the same time, the over-reduction of copper to its metallic state, generally identified as the H_2 oxidation site, thus affecting also the selectivity. Another interesting feature of nanosized copper-ceria catalysts is their easier desorption of carbon dioxide; this property is reflected into higher activity at low temperature, where CO_2 desorption is the rate-limiting step. An improved resistance toward the inhibiting effect of CO_2, typically present in the composition of the reformed stream, is a secondary but nonetheless beneficial effect.

Results reported above show that the ceria nanomorphology affects the catalytic properties as well as its dimension. It has been demonstrated that copper is preferentially dispersed onto defective planes, where copper-ceria interaction is boosted. Accordingly, catalysts prepared with specific morphologies are generally more active and selective.

The fundamental role of copper dispersion and its interaction with ceria is indirectly demonstrated by the development of "inverse" CeO_2/CuO catalysts. In these materials, ceria is deposited onto copper oxide; results clearly showed that the formation of nanostructures related to ceria and/or copper oxide, improving the contact points between the two oxides, is directly related to the catalytic activity and selectivity.

Deposition of both CeO_2 and CuO onto carbon-based supports intrinsically provides an intimate contact between copper and ceria. Moreover, the carbon-based supports offer large surface area, stable structure and they weaken the inhibiting effect of H_2O and CO_2 as they disadvantage their adsorption. It is worth noting that the optimal Ce/Cu ratio is around 1; evidently, the very small size of catalyst particles dispersed onto the support surface enhances the Cu-Ce distribution and interaction, thus also shifting the best composition to the equimolar ratio with respect to conventional CuO/CeO_2 catalysts.

Dopants also affect significantly the catalytic properties. In ceria-based catalysts, dopant addition is generally related to the modification of the redox properties and, in particular, to the improvement of bulk and/or surface oxygen vacancies. With regard to CuO/CeO_2 systems for CO-PROX, a larger number of oxygen vacancies is not straightforwardly linked to better catalytic performance. As a matter of fact, the improved redox properties should be coupled with a better copper dispersion in order to obtain more performing catalytic systems.

Figure 3.10 summarizes the above considerations.

Despite the absence of a general consensus on the exact nature of the active sites, the results reported in this chapter show that good catalysts based on CuO/CeO_2 for CO-PROX should have a copper-ceria interaction as wide as possible. Accordingly, the design of novel catalysts implies their engineering at the nanoscale level with the aim of a better utilization of the active components. Moreover, an opportune choice of additional components (dopants and/or supports as graphene and carbon

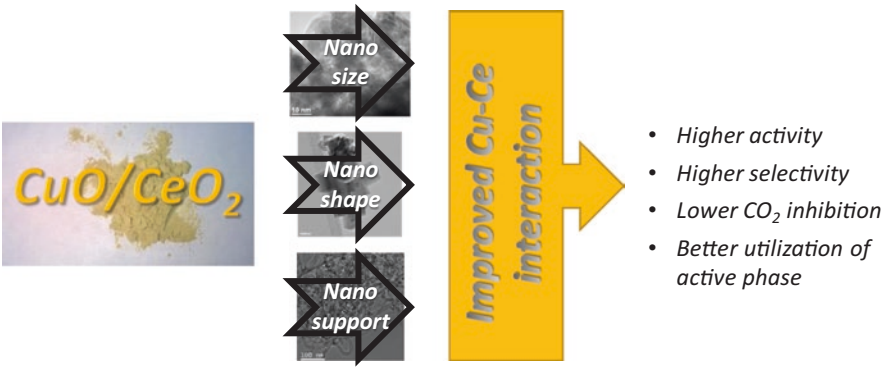

Fig. 3.10 How nanostructuring can affect the catalytic performance of CuO/CeO_2-based catalysts toward CO-PROX

nanotubes) can improve not only the intrinsic activity but also the resistance to the inhibiting effect of carbon dioxide and water vapor, unavoidable in reformate streams.

Finally, this chapter did not address the issue of structuring the active phase onto monolithic systems. However, structured catalysts are necessary under applicative conditions. Accordingly, another topic of interest is the development of active phases and preparation methods suitable for deposition onto substrates such as honeycombs, foams, and slabs.

References

1. D. Yadav, R. Banerjee, Economic assessment of hydrogen production from solar driven high-temperature steam electrolysis process. J. Clean. Prod. **183**, 1131–1155 (2018). https://doi.org/10.1016/j.jclepro.2018.01.074
2. K. Bareiß, C. de la Rua, M. Möckl, T. Hamacher, Life cycle assessment of hydrogen from proton exchange membrane water electrolysis in future energy systems. Appl. Energy **237**, 862–872 (2019). https://doi.org/10.1016/j.apenergy.2019.01.001
3. J. Moir, N. Soheilnia, P. O'Brien, A. Jelle, C.M. Grozea, D. Faulkner, M.G. Helander, G.A. Ozin, Enhanced hematite water electrolysis using a 3D antimony-doped tin oxide electrode. ACS Nano **7**, 4261–4274 (2013). https://doi.org/10.1021/nn400744d
4. E.C. Vagia, A.A. Lemonidou, Thermodynamic analysis of hydrogen production via autothermal steam reforming of selected components of aqueous bio-oil fraction. Int. J. Hydrog. Energy **33**, 2489–2500 (2008). https://doi.org/10.1016/j.ijhydene.2008.02.057
5. R. Rezaei, G. Moradi, Study of the performance of dry methane reforming in a microchannel reactor using sputtered Ni/Al2O3 coating on stainless steel. Int. J. Hydrog. Energy **43**, 21374–21385 (2018). https://doi.org/10.1016/j.ijhydene.2018.09.200
6. S. Kim, S.W. Yun, B. Lee, J. Heo, K. Kim, Y.T. Kim, H. Lim, Steam reforming of methanol for ultra-pure H2 production in a membrane reactor: techno-economic analysis. Int. J. Hydrog. Energy **44**, 2330–2339 (2018). https://doi.org/10.1016/j.ijhydene.2018.08.087

7. V. Fierro, O. Akdim, H. Provendier, C. Mirodatos, Ethanol oxidative steam reforming over Ni-based catalysts. J. Power Sources **145**, 659–666 (2005). https://doi.org/10.1016/j.jpowsour.2005.02.041
8. C.L. Muhich, B.D. Ehrhart, I. Al-Shankiti, B.J. Ward, C.B. Musgrave, A.W. Weimer, A review and perspective of efficient hydrogen generation via solar thermal water splitting. Wiley Interdiscip. Rev. Energ. Environ. **5**, 261–287 (2016). https://doi.org/10.1002/wene.174
9. G. Luciani, G. Landi, C. Imparato, G. Vitiello, F.A. Deorsola, A. Di Benedetto, A. Aronne, Improvement of splitting performance of Ce0.75Zr0.25O2 material: tuning bulk and surface properties by hydrothermal synthesis. Int. J. Hydrog. Energy **44**, 17565–17577 (2019). https://doi.org/10.1016/j.ijhydene.2019.05.021
10. P.M. Rao, I.S. Cho, X. Zheng, Flame synthesis of WO3 nanotubes and nanowires for efficient photoelectrochemical water-splitting. Proc. Combust. Inst. **34**, 2187–2195 (2013). https://doi.org/10.1016/j.proci.2012.06.122
11. A. Albarbar, M. Alrweq, *Proton Exchange Membrane Fuel Cells: Review* (Springer International Publishing, Cham, 2018)
12. E.D. Park, D. Lee, H.C. Lee, Recent progress in selective CO removal in a H2-rich stream. Catal. Today **139**, 280–290 (2009). https://doi.org/10.1016/j.cattod.2008.06.027
13. G. Ercolino, M.A. Ashraf, V. Specchia, S. Specchia, Performance evaluation and comparison of fuel processors integrated with PEM fuel cell based on steam or autothermal reforming and on CO preferential oxidation or selective methanation. Appl. Energy **143**, 138–153 (2015). https://doi.org/10.1016/j.apenergy.2014.12.088
14. M.A. Ashraf, G. Ercolino, S. Specchia, V. Specchia, Final step for CO syngas clean-up: comparison between CO-PROX and CO-SMET processes. Int. J. Hydrog. Energy **39**(31), 18109–18119 (2014)
15. Q. Zhang, L. Shore, R.J. Farrauto, Selective CO oxidation over a commercial PROX monolith catalyst for hydrogen fuel cell applications. Int. J. Hydrog. Energy **37**, 10874–10880 (2012). https://doi.org/10.1016/j.ijhydene.2012.04.032
16. F. Barrai, M.J. Castaldi, Experimental investigation of a JP8 fuel processor: autothermal reformer and CO-cleanup train. Ind. Eng. Chem. Res. **49**, 1577–1587 (2010). https://doi.org/10.1021/ie901735x
17. L. Du, J. Zhang, L. Sun, Z. Yuan, D. Li, A compact fuel processor integrated with 75kw PEM fuel cells, in *2011 International Conference on Electric Information and Control Engineering, ICEICE 2011—Proceedings. IEEE,* (2011), pp. 1906–1910
18. C. Fabiano, C. Italiano, A. Vita, L. Pino, M. Laganà, V. Recupero, Performance of 1.5 Nm3/h hydrogen generator by steam reforming of n-dodecane for naval applications. Int. J. Hydrog. Energy **41**, 19475–19483 (2016). https://doi.org/10.1016/j.ijhydene.2016.07.166
19. F. Cipitì, L. Pino, A. Vita, M. Laganà, V. Recupero, Performance of a 5 kWe fuel processor for polymer electrolyte fuel cells. Int. J. Hydrog. Energy **33**, 3197–3203 (2008). https://doi.org/10.1016/j.ijhydene.2008.02.042
20. A.B. Lamb, C.C. Scalione, G. Edgar, The preferential catalytic combustion of carbon monoxide in hydrogen. J. Am. Chem. Soc. **44**, 738–757 (1922). https://doi.org/10.1021/ja01425a007
21. W.E. Kuentzel, The preferential catalytic oxidation of carbon monoxide in the presence of hydrogen. I. The activity of two water gas conversion catalysts, of copper oxide, of manganese dioxide and of a mixture of these oxides. J. Am. Chem. Soc. **52**, 437–444 (1930). https://doi.org/10.1021/ja01365a001
22. W.E. Kuentzel, The preferential catalytic oxidation of carbon monoxide in the presence of hydrogen. II. The activity of 2-component hopcalites. J. Am. Chem. Soc. **52**, 445–455 (1930). https://doi.org/10.1021/ja01365a002
23. P.C. Liao, J.J. Carberry, T.H. Fleisch, E.E. Wolf, CO oxidation activity and XPS studies of PtCu γ-Al2O3 bimetallic catalysts. J. Catal. **74**, 307–316 (1982). https://doi.org/10.1016/0021-9517(82)90036-7
24. S. Akhter, J.M. White, The effect of oxygen islanding on Co and H2 oxidation on Pt(111). Surf. Sci. **171**, 527–542 (1986). https://doi.org/10.1016/0039-6028(86)91058-7

25. V. Gorodetskii, W. Drachsel, J.H. Block, The surface specificity of the oscillating CO oxidation on platinum investigated by field ion microscopy. Appl. Surf. Sci. **76–77**, 122–128 (1994). https://doi.org/10.1016/0169-4332(94)90332-8
26. A. Lesar, T. Yamanaka, Y. Ohno, T. Matsushima, Preferential occurrence of carbon monoxide oxidation on two reaction sites on platinum (113). Chem. Phys. Lett. **234**, 330–336 (1995). https://doi.org/10.1016/0009-2614(95)00061-8
27. G. Avgouropoulos, T. Ioannides, C. Papadopoulou, J. Batista, S. Hocevar, H.K. Matralis, A comparative study of Pt/γ-Al2O3, Au/α-Fe2O3 and CuO-CeO2 catalysts for the selective oxidation of carbon monoxide in excess hydrogen. Catal. Today **75**, 157–167 (2002). https://doi.org/10.1016/S0920-5861(02)00058-5
28. F. Mariño, C. Descorme, D. Duprez, Noble metal catalysts for the preferential oxidation of carbon monoxide in the presence of hydrogen (PROX). Appl. Catal. B Environ. **54**, 59–66 (2004). https://doi.org/10.1016/j.apcatb.2004.06.008
29. V. Recupero, L. Pino, A. Vita, F. Cipitì, M. Cordaro, M. Laganà, Development of a LPG fuel processor for PEFC systems: laboratory scale evaluation of autothermal reforming and preferential oxidation subunits. Int. J. Hydrog. Energy **30**, 963–971 (2005). https://doi.org/10.1016/j.ijhydene.2004.12.014
30. C.D. Dudfield, R. Chen, P.L. Adcock, A carbon monoxide PROX reactor for PEM fuel cell automotive application. Int. J. Hydrog. Energy **26**, 763–775 (2001). https://doi.org/10.1016/S0360-3199(00)00131-2
31. O. Görke, P. Pfeifer, Preferential CO oxidation over a platinum ceria alumina catalyst in a microchannel reactor. Int. J. Hydrog. Energy **36**, 4673–4681 (2011). https://doi.org/10.1016/j.ijhydene.2011.01.069
32. T.S. Nguyen, F. Morfin, M. Aouine, F. Bosselet, J.L. Rousset, L. Piccolo, Trends in the CO oxidation and PROX performances of the platinum-group metals supported on ceria. Catal. Today **253**, 106–114 (2015). https://doi.org/10.1016/j.cattod.2014.12.038
33. F. Morfin, T.S. Nguyen, J.L. Rousset, L. Piccolo, Synergy between hydrogen and ceria in Pt-catalyzed CO oxidation: an investigation on Pt–CeO2 catalysts synthesized by solution combustion. Appl. Catal. B Environ. **197**, 2–13 (2016). https://doi.org/10.1016/j.apcatb.2016.01.056
34. N. Bion, F. Epron, M. Moreno, F. Mariño, D. Duprez, Preferential oxidation of carbon monoxide in the presence of hydrogen (PROX) over noble metals and transition metal oxides: advantages and drawbacks. Top. Catal. **51**, 76–88 (2008). https://doi.org/10.1007/s11244-008-9116-x
35. S. Scirè, C. Crisafulli, S. Minicò, G.G. Condorelli, A. Di Mauro, Selective oxidation of CO in H2-rich stream over gold/iron oxide: an insight on the effect of catalyst pretreatment. J. Mol. Catal. A Chem. **284**, 24–32 (2008). https://doi.org/10.1016/j.molcata.2007.12.026
36. E. Quinet, F. Morfin, F. Diehl, P. Avenier, V. Caps, J.L. Rousset, Hydrogen effect on the preferential oxidation of carbon monoxide over alumina-supported gold nanoparticles. Appl. Catal. B Environ. **80**, 195–201 (2008). https://doi.org/10.1016/j.apcatb.2007.11.011
37. J.D.S.L. Fonseca, H.S. Ferreira, N. Bion, L. Pirault-Roy, M.D.C. Rangel, D. Duprez, F. Epron, Cooperative effect between copper and gold on ceria for CO-PROX reaction. Catal. Today **180**, 34–41 (2012). https://doi.org/10.1016/j.cattod.2011.06.008
38. A. Pitois, A. Pilenga, A. Pfrang, G. Tsotridis, Temperature-dependent CO desorption kinetics on supported gold nanoparticles: relevance to clean hydrogen production and fuel cell systems. Int. J. Hydrog. Energy **36**, 4375–4385 (2011). https://doi.org/10.1016/j.ijhydene.2010.12.123
39. P. Landon, J. Ferguson, B.E. Solsona, T. Garcia, A.F. Carley, A.A. Herzing, C.J. Kiely, S.E. Golunski, G.J. Hutchings, Selective oxidation of CO in the presence of H2, H2O and CO2 via gold for use in fuel cells. Chem. Commun., 3385–3387 (2005). https://doi.org/10.1039/b505295p
40. Y. Liu, B. Liu, Q. Wang, C. Li, W. Hu, Y. Liu, P. Jing, W. Zhao, J. Zhang, Three-dimensionally ordered macroporous Au/CeO2-Co 3O4 catalysts with mesoporous walls for enhanced CO

preferential oxidation in H2-rich gases. J. Catal. **296**, 65–76 (2012). https://doi.org/10.1016/j.jcat.2012.09.003
41. P. Lakshmanan, J.E. Park, E.D. Park, Recent advances in preferential oxidation of CO in H2 over gold catalysts. Catal. Surv. Asia **18**, 75–88 (2014)
42. T. Cwele, N. Mahadevaiah, S. Singh, H.B. Friedrich, Effect of Cu additives on the performance of a cobalt substituted ceria (Ce0.90Co0.10O2-δ) catalyst in total and preferential CO oxidation. Appl. Catal. B Environ. **182**, 1–14 (2016). https://doi.org/10.1016/j.apcatb.2015.08.043
43. C.A. Chagas, E.F. de Souza, R.L. Manfro, S.M. Landi, M.M.V.M. Souza, M. Schmal, Copper as promoter of the NiO-CeO2 catalyst in the preferential CO oxidation. Appl. Catal. B Environ. **182**, 257–265 (2016). https://doi.org/10.1016/j.apcatb.2015.09.033
44. C.G. Maciel, M.N. Belgacem, J.M. Assaf, Performance of CuO-CeO2 catalysts with low copper content in CO preferential oxidation reaction. Catal. Letters **141**, 316–321 (2011). https://doi.org/10.1007/s10562-010-0486-x
45. E. Moretti, L. Storaro, A. Talon, M. Lenarda, One-pot mesoporous Al-Ce-Cu oxide systems as catalysts for the preferential carbon monoxide oxidation (CO-PROX). Catal. Commun. **10**, 522–527 (2009). https://doi.org/10.1016/j.catcom.2008.10.023
46. A. Martínez-Arias, D. Gamarra, M. Fernández-García, A. Hornés, P. Bera, Z. Koppány, Z. Schay, Redox-catalytic correlations in oxidised copper-ceria CO-PROX catalysts. Catal. Today **143**, 211–217 (2009). https://doi.org/10.1016/j.cattod.2008.09.018
47. D. Gamarra, G. Munuera, A.B. Hungría, M. Fernández-García, J.C. Conesa, P.A. Midgley, X.Q. Wang, J.C. Hanson, J.A. Rodríguez, A. Martínez-Arias, Structure-activity relationship in nanostructured copper-ceria-based preferential CO oxidation catalysts. J. Phys. Chem. C **111**, 11026–11038 (2007). https://doi.org/10.1021/jp072243k
48. T. Caputo, L. Lisi, R. Pirone, G. Russo, On the role of redox properties of CuO/CeO2 catalysts in the preferential oxidation of CO in H2-rich gases. Appl. Catal. A Gen. **348**, 42–53 (2008). https://doi.org/10.1016/j.apcata.2008.06.025
49. A. Di Benedetto, G. Landi, L. Lisi, G. Russo, Role of CO2 on CO preferential oxidation over CuO/CeO2 catalyst. Appl. Catal. B Environ. **142–143**, 169–177 (2013). https://doi.org/10.1016/j.apcatb.2013.05.001
50. J.A. Cecilia, A. Arango-Díaz, F. Franco, J. Jiménez-Jiménez, L. Storaro, E. Moretti, E. Rodríguez-Castellón, CuO-CeO<inf>2</inf> supported on montmorillonite-derived porous clay heterostructures (PCH) for preferential CO oxidation in H<inf>2</inf>−rich stream. Catal. Today **253**, 126–136 (2015). https://doi.org/10.1016/j.cattod.2015.01.040
51. X. Guo, J. Li, R. Zhou, Catalytic performance of manganese doped CuO-CeO2 catalysts for selective oxidation of CO in hydrogen-rich gas. Fuel **163**, 56–64 (2016). https://doi.org/10.1016/j.fuel.2015.09.043
52. W.W. Wang, P.P. Du, S.H. Zou, H.Y. He, R.X. Wang, Z. Jin, S. Shi, Y.Y. Huang, R. Si, Q.S. Song, C.J. Jia, C.H. Yan, Highly dispersed copper oxide clusters as active species in copper-ceria catalyst for preferential oxidation of carbon monoxide. ACS Catal. **5**, 2088–2099 (2015). https://doi.org/10.1021/cs5014909
53. J.S. Elias, N. Artrith, M. Bugnet, L. Giordano, G.A. Botton, A.M. Kolpak, Y. Shao-Horn, Elucidating the nature of the active phase in copper/ceria catalysts for CO oxidation. ACS Catal. **6**, 1675–1679 (2016). https://doi.org/10.1021/acscatal.5b02666
54. A. Davó-Quiñonero, M. Navlani-García, D. Lozano-Castelló, A. Bueno-López, J.A. Anderson, Role of hydroxyl groups in the preferential oxidation of CO over copper oxide–cerium oxide catalysts. ACS Catal. **6**, 1723–1731 (2016). https://doi.org/10.1021/acscatal.5b02741
55. A. Di Benedetto, G. Landi, L. Lisi, CO reactive adsorption at low temperature over CuO/CeO2structured catalytic monolith. Int. J. Hydrog. Energy **42**, 12262–12275 (2017). https://doi.org/10.1016/j.ijhydene.2017.03.077
56. A. Arango-Díaz, J.A. Cecilia, L. Dos Santos-Gómez, D. Marrero-López, E.R. Losilla, J. Jiménez-Jiménez, E. Rodríguez-Castellón, Characterization and performance in preferential oxidation of CO of CuO-CeO2 catalysts synthesized using polymethyl metac-

rylate (PMMA) as template. Int. J. Hydrog. Energy **40**, 11254–11260 (2015). https://doi.org/10.1016/j.ijhydene.2015.04.094
57. C. Xu, S. Li, Y. Zhang, Y. Li, J. Zhou, G. Qin, Synthesis of CuO x –CeO 2 catalyst with high-density interfaces for selective oxidation of CO in H 2 -rich stream. Int. J. Hydrog. Energy **44**, 4156–4166 (2019). https://doi.org/10.1016/j.ijhydene.2018.12.152
58. J. Ding, L. Li, H. Li, S. Chen, S. Fang, T. Feng, G. Li, Optimum preferential oxidation performance of CeO 2 -CuO x -RGO composites through interfacial regulation. ACS Appl. Mater. Interfaces **10**, 7935–7945 (2018). https://doi.org/10.1021/acsami.7b15549
59. X. Liu, X. Li, H. Qian, J. Chi, B. Chen, S. Wang, C. Chen, N. Zhang, Preferential CO oxidation over CuO–CeO 2 catalyst synthesized from MOF with nitrogen-containing ligand as precursor. Int. J. Hydrog. Energy **43**, 23299–23309 (2018). https://doi.org/10.1016/j.ijhydene.2018.10.162
60. W. Hu, G. Li, J. Chen, F. Huang, M. Gong, L. Zhong, Y. Chen, Enhancement of activity and hydrothermal stability of Pd/ZrO2-Al2O3 doped by Mg for methane combustion under lean conditions. Fuel **194**, 368–374 (2017). https://doi.org/10.1016/j.fuel.2016.11.028
61. J. Lu, J. Wang, Q. Zou, D. He, L. Zhang, Z. Xu, S. He, Y. Luo, Unravelling the nature of the active species as well as the doping effect over Cu/Ce-based catalyst for carbon monoxide preferential oxidation. ACS Catal. **9**, 2177–2195 (2019). https://doi.org/10.1021/acscatal.8b04035
62. X. Zhang, X. Zhang, L. Song, F. Hou, Y. Yang, Y. Wang, N. Liu, Enhanced catalytic performance for CO oxidation and preferential CO oxidation over CuO/CeO2 catalysts synthesized from metal organic framework: effects of preparation methods. Int. J. Hydrog. Energy **43**, 18279–18288 (2018). https://doi.org/10.1016/j.ijhydene.2018.08.060
63. H. Choi, J. Kim, S.J. Choung, J. Kim, M.R. Othman, Complete removal of carbon monoxide by functional nanoparticles for hydrogen fuel cell application. Chem. Eng. Sci. **172**, 688–693 (2017). https://doi.org/10.1016/j.ces.2017.07.026
64. M. Konsolakis, The role of Copper–Ceria interactions in catalysis science: recent theoretical and experimental advances. Appl. Catal. B Environ. **198**, 49–66 (2016). https://doi.org/10.1016/j.apcatb.2016.05.037
65. S. Scirè, C. Crisafulli, P.M. Riccobene, G. Patanè, A. Pistone, Selective oxidation of CO in H 2-rich stream over Au/CeO 2 and Cu/CeO 2 catalysts: an insight on the effect of preparation method and catalyst pretreatment. Appl. Catal. A Gen. **417–418**, 66–75 (2012). https://doi.org/10.1016/j.apcata.2011.12.025
66. A. Di Benedetto, G. Landi, L. Lisi, Improved CO-PROX performance of CuO/CeO2 catalysts by using nanometric ceria as support. Catalysts **8**, 209 (2018). https://doi.org/10.3390/catal8050209
67. A.P. Jia, G.S. Hu, L. Meng, Y.L. Xie, J.Q. Lu, M.F. Luo, CO oxidation over CuO/Ce 1-xCu xO 2-δ and Ce 1-xCu xO 2-δ catalysts: synergetic effects and kinetic study. J. Catal. **289**, 199–209 (2012). https://doi.org/10.1016/j.jcat.2012.02.010
68. D. Gu, C.J. Jia, H. Bongard, B. Spliethoff, C. Weidenthaler, W. Schmidt, F. Schüth, Ordered mesoporous Cu-Ce-O catalysts for CO preferential oxidation in H2-rich gases: influence of copper content and pretreatment conditions. Appl. Catal. B Environ. **152–153**, 11–18 (2014). https://doi.org/10.1016/j.apcatb.2014.01.011
69. D. Gamarra, C. Belver, M. Fernández-García, A. Martínez-Arias, Selective CO oxidation in excess H2 over copper-ceria catalysts: identification of active entities/species. J. Am. Chem. Soc. **129**, 12064–12065 (2007). https://doi.org/10.1021/ja073926g
70. A. Gurbani, J.L. Ayastuy, M.P. González-Marcos, M.A. Gutiérrez-Ortiz, CuO-CeO 2 catalysts synthesized by various methods: comparative study of redox properties. Int. J. Hydrog. Energy **35**, 11582–11590 (2010). https://doi.org/10.1016/j.ijhydene.2010.04.045
71. J. Wang, H. Pu, G. Wan, K. Chen, J. Lu, Y. Lei, L. Zhong, S. He, C. Han, Y. Luo, Promoted the reduction of Cu2+ to enhance CuO–CeO2 catalysts for CO preferential oxidation in H2-rich streams: effects of preparation methods and copper precursors. Int. J. Hydrog. Energy **42**, 21955–21968 (2017). https://doi.org/10.1016/j.ijhydene.2017.07.122

72. P.S. Barbato, S. Colussi, A. Di Benedetto, G. Landi, L. Lisi, J. Llorca, A. Trovarelli, Origin of high activity and selectivity of CuO/CeO_2 catalysts prepared by solution combustion synthesis in CO-PROX reaction. J. Phys. Chem. C **120**, 13039–13048 (2016). https://doi.org/10.1021/acs.jpcc.6b02433
73. G. Avgouropoulos, T. Ioannides, Selective CO oxidation over CuO-CeO2 catalysts prepared via the urea-nitrate combustion method. Appl. Catal. A Gen. **244**, 155–167 (2003). https://doi.org/10.1016/S0926-860X(02)00558-6
74. J. Papavasiliou, J. Vakros, G. Avgouropoulos, Impact of acid treatment of CuO-CeO2 catalysts on the preferential oxidation of CO reaction. Catal. Commun. **115**, 68–72 (2018). https://doi.org/10.1016/j.catcom.2018.07.014
75. J. Papavasiliou, M. Rawski, J. Vakros, G. Avgouropoulos, A novel post-synthesis modification of CuO-CeO2 catalysts: effect on their activity for selective CO oxidation. ChemCatChem **10**, 2096–2106 (2018). https://doi.org/10.1002/cctc.201701968
76. P.P. Du, W.W. Wang, C.J. Jia, Q.S. Song, Y.Y. Huang, R. Si, Effect of strongly bound copper species in copper-ceria catalyst for preferential oxidation of carbon monoxide. Appl. Catal. A Gen. **518**, 87–101 (2016). https://doi.org/10.1016/j.apcata.2015.10.041
77. A. Martínez-Arias, A.B. Hungría, G. Munuera, D. Gamarra, Preferential oxidation of CO in rich H2 over CuO/CeO2: details of selectivity and deactivation under the reactant stream. Appl. Catal. B Environ. **65**, 207–216 (2006). https://doi.org/10.1016/j.apcatb.2006.02.003
78. H.C. Lee, D.H. Kim, Kinetics of CO and H2 oxidation over CuO-CeO2 catalyst in H2 mixtures with CO2 and H2O. Catal. Today **132**, 109–116 (2008). https://doi.org/10.1016/j.cattod.2007.12.028
79. X. Guo, J. Mao, R. Zhou, Influence of the copper coverage on the dispersion of copper oxide and the catalytic performance of CuO/CeO2(rod) catalysts in preferential oxidation of CO in excess hydrogen. J. Power Sources **371**, 119–128 (2017). https://doi.org/10.1016/j.jpowsour.2017.10.055
80. P.S. Barbato, S. Colussi, A. Di Benedetto, G. Landi, L. Lisi, J. Llorca, A. Trovarelli, CO preferential oxidation under H2-rich streams on copper oxide supported on Fe promoted CeO2. Appl. Catal. A Gen. **506**, 268–277 (2015). https://doi.org/10.1016/j.apcata.2015.09.018
81. A. Lopez Cámara, V. Cortés Corberán, L. Barrio, G. Zhou, R. Si, J.C. Hanson, M. Monte, J.C. Conesa, J.A. Rodriguez, A. Martínez-Arias, Improving the CO-PROX performance of inverse CeO2/CuO catalysts: doping of the CuO component with Zn. J. Phys. Chem. C **118**, 9030–9041 (2014). https://doi.org/10.1021/jp5009384
82. A. Kubacka, A. Martínez-Arias, M. Fernández-García, Role of the interface in base-metal ceria-based catalysts for hydrogen purification and production processes. ChemCatChem **7**, 3614–3624 (2015). https://doi.org/10.1002/cctc.201500593
83. A. Trovarelli, J. Llorca, Ceria catalysts at nanoscale: how do crystal shapes shape catalysis? ACS Catal. **7**, 4716–4735 (2017)
84. G.R. Kosmambetova, Structural organization of nanophase catalysts for preferential CO oxidation. Theor. Exp. Chem. **50**, 265–281 (2014). https://doi.org/10.1007/s11237-014-9376-4
85. I. López, T. Valdés-Solís, G. Marbán, An attempt to rank copper-based catalysts used in the CO-PROX reaction. Int. J. Hydrog. Energy **33**, 197–205 (2008). https://doi.org/10.1016/j.ijhydene.2007.09.011
86. C.G. MacIel, T.D.F. Silva, M.I. Hirooka, M.N. Belgacem, J.M. Assaf, Effect of nature of ceria support in CuO/CeO 2 catalyst for PROX-CO reaction. Fuel **97**, 245–252 (2012). https://doi.org/10.1016/j.fuel.2012.02.004
87. R. Zhang, J.T. Miller, C.D. Baertsch, Identifying the active redox oxygen sites in a mixed Cu and Ce oxide catalyst by in situ X-ray absorption spectroscopy and anaerobic reactions with CO in concentrated H2. J. Catal. **294**, 69–78 (2012). https://doi.org/10.1016/j.jcat.2012.07.005
88. V.D. Araújo, W. Avansi, A.J.S. Mascarenhas, H.M.C. Andrade, E. Longo, M.I.B. Bernardi, Ce0.97Cu0.03O2 nanocatalysts synthesized via microwave-assisted hydrothermal method:

characterization and CO-PROX catalytic efficiency. Earth Environ. Sci. Trans. R Soc. Edinburgh **1552**, 17–22 (2013). https://doi.org/10.1557/opl.2013.588
89. A. Arango-Díaz, E. Moretti, A. Talon, L. Storaro, M. Lenarda, P. Núñez, J. Marrero-Jerez, J. Jiménez-Jiménez, A. Jiménez-López, E. Rodríguez-Castellón, Preferential CO oxidation (CO-PROX) catalyzed by CuO supported on nanocrystalline CeO2 prepared by a freeze-drying method. Appl. Catal. A Gen. **477**, 54–63 (2014). https://doi.org/10.1016/j.apcata.2014.02.033
90. H. Yen, Y. Seo, S. Kaliaguine, F. Kleitz, Tailored mesostructured copper/ceria catalysts with enhanced performance for preferential oxidation of CO at low temperature. Angew Chemie Int. Ed. **51**, 12032–12035 (2012). https://doi.org/10.1002/anie.201206505
91. F. Zhang, C. Chen, W.M. Xiao, L. Xu, N. Zhang, CuO/CeO2 catalysts with well-dispersed active sites prepared from Cu 3 (BTC) 2 metal-organic framework precursor for preferential CO oxidation. Catal. Commun. **26**, 25–29 (2012). https://doi.org/10.1016/j.catcom.2012.04.028
92. S.H. Wang, L. Xu, P. Shen, C. Chen, N. Zhang, New approach to synthesis of CuO/CeO2 catalysts for preferential CO oxidation. Appl. Mech. Mater., 666–670 (2014)
93. X. Li, X.Y. Quek, D.A.J. Michel Ligthart, M. Guo, Y. Zhang, C. Li, Q. Yang, E.J.M. Hensen, CO-PROX reactions on copper cerium oxide catalysts prepared by melt infiltration. Appl. Catal. B Environ. **123–124**, 424–432 (2012). https://doi.org/10.1016/j.apcatb.2012.05.009
94. C. Tang, J. Sun, X. Yao, Y. Cao, L. Liu, C. Ge, F. Gao, L. Dong, Efficient fabrication of active CuO-CeO2/SBA-15 catalysts for preferential oxidation of CO by solid state impregnation. Appl. Catal. B Environ. **146**, 201–212 (2014). https://doi.org/10.1016/j.apcatb.2013.05.060
95. L. Gong, Z. Huang, L. Luo, N. Zhang, Promoting effect of MnOx on the performance of CuO/CeO2 catalysts for preferential oxidation of CO in H2-rich gases. React. Kinet. Mech. Catal. **111**, 489–504 (2014). https://doi.org/10.1007/s11144-013-0662-2
96. S. Zeng, T. Chen, K. Liu, H. Su, Promotion effect of metal oxides on inverse CeO2/CuO catalysts for preferential oxidation of CO. Catal. Commun. **45**, 16–20 (2014). https://doi.org/10.1016/j.catcom.2013.10.022
97. Z. Liu, J. Chen, R. Zhou, X. Zheng, Influence of ethanol washing in precursor on CuO-CeO2 catalysts in preferential oxidation of CO in excess hydrogen. Catal. Letters **123**, 102–106 (2008). https://doi.org/10.1007/s10562-008-9401-0
98. L.C. Chung, C.T. Yeh, Synthesis of highly active CuO-CeO2 nanocomposites for preferential oxidation of carbon monoxide at low temperatures. Catal. Commun. **9**, 670–674 (2008). https://doi.org/10.1016/j.catcom.2007.07.041
99. G. Marbán, I. López, T. Valdés-Solís, Preferential oxidation of CO by CuOx/CeO2 nanocatalysts prepared by SACOP. Mechanisms of deactivation under the reactant stream. Appl. Catal. A Gen. **361**, 160–169 (2009). https://doi.org/10.1016/j.apcata.2009.04.014
100. G. Sedmak, S. Hočevar, J. Levec, Kinetics of selective CO oxidation in excess of H2 over the nanostructured Cu0.1Ce0.9O2-y catalyst. J. Catal. **213**, 135–150 (2003). https://doi.org/10.1016/S0021-9517(02)00019-2
101. S. Xu, D. Sun, H. Liu, X. Wang, X. Yan, Fabrication of Cu-doped cerium oxide nanofibers via electrospinning for preferential CO oxidation. Catal. Commun. **12**, 514–518 (2011). https://doi.org/10.1016/j.catcom.2010.11.021
102. C. Borchers, M.L. Martin, G.A. Vorobjeva, O.S. Morozova, A.A. Firsova, A.V. Leonov, E.Z. Kurmaev, A.I. Kukharenko, I.S. Zhidkov, S.O. Cholakh, Cu–CeO2 nanocomposites: mechanochemical synthesis, physico-chemical properties, CO-PROX activity. J. Nanopart. Res. **18**, 344 (2016). https://doi.org/10.1007/s11051-016-3640-6
103. J. Han, H.J. Kim, S. Yoon, H. Lee, Shape effect of ceria in Cu/ceria catalysts for preferential CO oxidation. J. Mol. Catal. A Chem. **335**, 82–88 (2011). https://doi.org/10.1016/j.molcata.2010.11.017
104. M. Monte, D. Gamarra, A. López Cámara, S.B. Rasmussen, N. Gyorffy, Z. Schay, A. Martínez-Arias, J.C. Conesa, Preferential oxidation of CO in excess H2 over CuO/CeO2

catalysts: performance as a function of the copper coverage and exposed face present in the CeO2 support. Catal. Today **229**, 104–113 (2014)
105. D. Gamarra, A.L. Cámara, M. Monte, S.B. Rasmussen, L.E. Chinchilla, A.B. Hungría, G. Munuera, N. Gyorffy, Z. Schay, V.C. Corberán, J.C. Conesa, A. Martínez-Arias, Preferential oxidation of CO in excess H2 over CuO/CeO2 catalysts: characterization and performance as a function of the exposed face present in the CeO2 support. Appl. Catal. B Environ. **130–131**, 224–238 (2013). https://doi.org/10.1016/j.apcatb.2012.11.008
106. X. Guo, R. Zhou, A new insight into the morphology effect of ceria on CuO/CeO2catalysts for CO selective oxidation in hydrogen-rich gas. Cat. Sci. Technol. **6**, 3862–3871 (2016). https://doi.org/10.1039/c5cy01816a
107. Y. Xie, J. Wu, G. Jing, H. Zhang, S. Zeng, X. Tian, X. Zou, J. Wen, H. Su, C.J. Zhong, P. Cui, Structural origin of high catalytic activity for preferential CO oxidation over CuO/CeO2 nanocatalysts with different shapes. Appl. Catal. B Environ. **239**, 665–676 (2018). https://doi.org/10.1016/j.apcatb.2018.08.066
108. T. Kou, C. Si, J. Pinto, C. Ma, Z. Zhang, Dealloying assisted high-yield growth of surfactant-free <110> highly active Cu-doped CeO 2 nanowires for low-temperature CO oxidation. Nanoscale **9**, 8007–8014 (2017). https://doi.org/10.1039/c7nr02405c
109. X. Gong, B. Liu, B. Kang, G. Xu, Q. Wang, C. Jia, J. Zhang, Boosting Cu-Ce interaction in CuxO/CeO2 nanocube catalysts for enhanced catalytic performance of preferential oxidation of CO in H2-rich gases. Mol. Catal. **436**, 90–99 (2017). https://doi.org/10.1016/j.mcat.2017.04.013
110. A. Hornés, A.B. Hungría, P. Bera, A. López Cámara, M. Fernández-García, A. Martínez-Arias, L. Barrio, M. Estrella, G. Zhou, J.J. Fonseca, J.C. Hanson, J.A. Rodriguez, Inverse CeO2/CuO catalyst as an alternative to classical direct configurations for preferential oxidation of CO in hydrogen-rich stream. J. Am. Chem. Soc. **132**, 34–35 (2010). https://doi.org/10.1021/ja9089846
111. S. Zeng, K. Liu, T. Chen, H. Su, Influence of crystallite size and interface on the catalytic performance over the CeO2/CuO catalysts. Int. J. Hydrog. Energy **38**, 14542–14549 (2013). https://doi.org/10.1016/j.ijhydene.2013.09.023
112. S. Zeng, W. Zhang, M. Śliwa, H. Su, Comparative study of CeO2/CuO and CuO/CeO2 catalysts on catalytic performance for preferential CO oxidation. Int. J. Hydrog. Energy **38**, 3597–3605 (2013). https://doi.org/10.1016/j.ijhydene.2013.01.030
113. S.H. Zeng, T.J. Chen, H.Q. Su, Q. Man, W.L. Zhang, CeO2/CuO catalysts with Na2CO3 as precipitant for preferential oxidation of CO. Adv. Mater. Res **805-806**, 1297–1301 (2013)
114. S. Zeng, Y. Wang, B. Qin, X. Gu, H. Su, L. Li, K. Liu, Inverse CeO2/CuO catalysts prepared by different precipitants for preferential CO oxidation in hydrogen-rich streams. Cat. Sci. Technol. **3**, 3163–3172 (2013). https://doi.org/10.1039/c3cy00478c
115. S. Zeng, W. Zhang, N. Liu, H. Su, Inverse CeO2/CuO catalysts prepared by hydrothermal method for preferential CO oxidation. Catal. Letters **143**, 1018–1024 (2013). https://doi.org/10.1007/s10562-013-1065-8
116. S. Zeng, Y. Wang, K. Liu, F. Liu, H. Su, CeO 2 nanoparticles supported on CuO with petal-like and sphere-flower morphologies for preferential CO oxidation. Int. J. Hydrog. Energy **37**, 11640–11649 (2012). https://doi.org/10.1016/j.ijhydene.2012.05.086
117. S. Zeng, Y. Wang, S. Ding, J.J.H.B. Sattler, E. Borodina, L. Zhang, B.M. Weckhuysen, H. Su, Active sites over CuO/CeO2 and inverse CeO2/CuO catalysts for preferential CO oxidation. J. Power Sources **256**, 301–311 (2014). https://doi.org/10.1016/j.jpowsour.2014.01.098
118. S. Zeng, K. Liu, L. Zhang, B. Qin, T. Chen, Y. Yin, H. Su, Deactivation analyses of CeO2/CuO catalysts in the preferential oxidation of carbon monoxide. J. Power Sources **261**, 46–54 (2014). https://doi.org/10.1016/j.jpowsour.2014.03.043
119. A. López Cámara, V. Cortés Corberán, L. Barrio, G. Zhou, R. Si, J.C. Hanson, M. Monte, J.C. Conesa, J.A. Rodriguez, A. Martínez-Arias, Improving the CO-PROX performance of inverse CeO2/CuO catalysts: doping of the CuO component with Zn. J. Phys. Chem. C **118**, 9030–9041 (2014). https://doi.org/10.1021/jp5009384

120. S. Chen, L. Li, W. Hu, X. Huang, Q. Li, Y. Xu, Y. Zuo, G. Li, Anchoring high-concentration oxygen vacancies at interfaces of CeO2-x/Cu toward enhanced activity for preferential CO oxidation. ACS Appl. Mater. Interfaces **7**, 22999–23007 (2015). https://doi.org/10.1021/acsami.5b06302
121. C. Gu, R. Qi, Y. Wei, X. Zhang, Preparation and performances of nanorod-like inverse CeO2–CuO catalysts derived from Ce-1,3,5-Benzene tricarboxylic acid for CO preferential oxidation. React. Kinet. Mech. Catal. **124**, 651–667 (2018). https://doi.org/10.1007/s11144-018-1374-4
122. Y. Xie, Y. Yin, S. Zeng, M. Gao, H. Su, Coexistence of Cu+ and Cu2+ in star-shaped CeO2/CuxO catalyst for preferential CO oxidation. Catal. Commun. **99**, 110–114 (2017). https://doi.org/10.1016/j.catcom.2017.06.003
123. C. Chen, R. Wang, P. Shen, D. Zhao, N. Zhang, Inverse CeO2/CuO catalysts prepared from heterobimetallic metal-organic framework precursor for preferential CO oxidation in H2-rich stream. Int. J. Hydrog. Energy **40**, 4830–4839 (2015). https://doi.org/10.1016/j.ijhydene.2015.02.066
124. S. Zeng, L. Zhang, N. Jiang, M. Gao, X. Zhao, Y. Yin, H. Su, Multi-wall carbon nanotubes as support of copper-cerium composite for preferential oxidation of carbon monoxide. J. Power Sources **293**, 1016–1023 (2015). https://doi.org/10.1016/j.jpowsour.2015.04.115
125. Y. Gao, K. Xie, W. Wang, S. Mi, N. Liu, G. Pan, W. Huang, Structural features and catalytic performance in CO preferential oxidation of CuO-CeO2 supported on multi-walled carbon nanotubes. Cat. Sci. Technol. **5**, 1568–1579 (2015). https://doi.org/10.1039/c4cy01220h
126. A.B. Dongil, B. Bachiller-Baeza, E. Castillejos, N. Escalona, A. Guerrero-Ruiz, I. Rodríguez-Ramos, The promoter effect of potassium in CuO/CeO2 systems supported on carbon nanotubes and graphene for the CO-PROX reaction. Cat. Sci. Technol. **6**, 6118–6127 (2016). https://doi.org/10.1039/C6CY00304D
127. H. Zhang, C. Xu, J. Ding, H. Su, S. Zeng, RGO/MWCNTs/Cu x O-CeO2 ternary nanocomposites for preferential CO oxidation in hydrogen-rich streams. Appl. Surf. Sci. **426**, 50–55 (2017). https://doi.org/10.1016/j.apsusc.2017.07.154
128. C. Xu, S. Zeng, H. Zhang, Y. Xie, A. Zhang, G. Jing, H. Su, Facile hydrothermal procedure to synthesize sheet-on-sheet reduced graphene oxide (RGO)/Cu x O[sbnd]CeO2 nanocomposites for preferential oxidation of carbon monoxide. Int. J. Hydrog. Energy **42**, 14133–14143 (2017). https://doi.org/10.1016/j.ijhydene.2017.04.058
129. D. Zhang, J. Qin, D. Wei, S. Yang, S. Wang, C. Hu, Enhancing the CO preferential oxidation (CO-PROX) of CuO–CeO2/reduced graphene oxide (rGO) by conductive rGO-wrapping based on the interfacial charge transfer. Catal. Letters **148**, 3454–3466 (2018). https://doi.org/10.1007/s10562-018-2520-3
130. L. Shi, G. Zhang, Y. Wang, Tailoring catalytic performance of carbon nanotubes confined CuO–CeO2 catalysts for CO preferential oxidation. Int. J. Hydrog. Energy **43**, 18211–18219 (2018). https://doi.org/10.1016/j.ijhydene.2018.08.020
131. A. Martínez-Arias, M. Fernández-García, O. Gálvez, J.M. Coronado, J.A. Anderson, J.C. Conesa, J. Soria, G. Munuera, Comparative study on redox properties and catalytic behavior for CO oxidation of CuO/CeO2 and CuO/ZrCeO4 catalysts. J. Catal. **195**, 207–216 (2000). https://doi.org/10.1006/jcat.2000.2981
132. L.H. Reddy, G.K. Reddy, D. Devaiah, B.M. Reddy, A rapid microwave-assisted solution combustion synthesis of CuO promoted CeO2 -M x O y (M = Zr, La, Pr and Sm) catalysts for CO oxidation. Appl. Catal. A Gen. **445–446**, 297–305 (2012). https://doi.org/10.1016/j.apcata.2012.08.024
133. T. Caputo, R. Pirone, G. Russo, Supported CuO/Ce1-x Zr x O2 catalysts for the preferential oxidation of CO in H2-rich gases. Kinet. Catal. **47**, 756–764 (2006). https://doi.org/10.1134/S0023158406050156
134. J.L. Ayastuy, A. Gurbani, M.P. González-Marcos, M.A. Gutiérrez-Ortiz, Selective CO oxidation in H2 streams on CuO/Ce xZr 1-xO 2 catalysts: correlation between activity and low tem-

perature reducibility. Int. J. Hydrog. Energy **37**, 1993–2006 (2012). https://doi.org/10.1016/j.ijhydene.2011.04.178
135. J. Wang, L. Deng, D. He, J. Lu, S. He, S. He, Y. Luo, A facile and rapid route to synthesize CuO<inf>x</inf>/Ce<inf>0.8</inf>Zr<inf>0.2</inf>O<inf>2</inf> catalysts with high performance for CO preferential oxidation (CO-PROX). Int. J. Hydrog. Energy **40**, 12478–12488 (2015). https://doi.org/10.1016/j.ijhydene.2015.07.063
136. X. Guo, Z. Qiu, J. Mao, R. Zhou, Doping effect of transition metals (Zr, Mn, Ti and Ni) on well-shaped CuO/CeO 2 (rods): nano/micro structure and catalytic performance for selective oxidation of CO in excess H2. Phys. Chem. Chem. Phys. **20**, 25983–25994 (2018). https://doi.org/10.1039/c8cp03696a
137. H. Jin, R. You, S. Zhou, K. Ma, M. Meng, L. Zheng, J. Zhang, T. Hu, In-situ DRIFTS and XANES identification of copper species in the ternary composite oxide catalysts CuMnCeO during CO preferential oxidation. Int. J. Hydrog. Energy **40**, 3919–3931 (2015). https://doi.org/10.1016/j.ijhydene.2015.01.086
138. J.A. Cecilia, A. Arango-Díaz, V. Rico-Pérez, A. Bueno-López, E. Rodríguez-Castellón, The influence of promoters (Zr, La, Tb, Pr) on the catalytic performance of CuO-CeO<inf>2</inf> systems for the preferential oxidation of CO in the presence of CO<inf>2</inf> and H<inf>2</inf>O. Catal. Today **253**, 115–125 (2015). https://doi.org/10.1016/j.cattod.2015.02.012
139. J.E. De Oliveira, S. Rico-Francés, Z. Abdelouahab-Reddam, F. Coloma, J. Silvestre-Albero, A. Sepúlveda-Escribano, E.V. Ramos-Fernandez, High performance of Cu/CeO<inf>2</inf>-Nb<inf>2</inf>O<inf>5</inf> catalysts for preferential CO oxidation and total combustion of toluene. Appl. Catal. A Gen. **502**, 129–137 (2015). https://doi.org/10.1016/j.apcata.2015.05.033
140. J. Kugai, T. Moriya, S. Seino, T. Nakagawa, Y. Ohkubo, H. Nitani, Y. Mizukoshi, T.A. Yamamoto, Effect of support for PtCu bimetallic catalysts synthesized by electron beam irradiation method on preferential CO oxidation. Appl. Catal. B Environ. **126**, 306–314 (2012). https://doi.org/10.1016/j.apcatb.2012.07.028
141. J. Kugai, T. Moriya, S. Seino, T. Nakagawa, Y. Ohkubo, H. Nitani, H. Daimon, T.A. Yamamoto, CeO 2-supported Pt-Cu alloy nanoparticles synthesized by radiolytic process for highly selective CO oxidation. Int. J. Hydrog. Energy **37**, 4787–4797 (2012). https://doi.org/10.1016/j.ijhydene.2011.12.070
142. J. Kugai, T. Moriya, S. Seino, T. Nakagawa, Y. Ohkubo, H. Nitani, T. Akita, Y. Mizukoshi, T.A. Yamamoto, Effect of CeO2 support properties on structure of Pt-Cu nanoparticles synthesized by electron beam irradiation method for preferential CO oxidation. Chem. Eng. J. **223**, 347–355 (2013). https://doi.org/10.1016/j.cej.2013.02.116
143. S. Lang, M. Türk, B. Kraushaar-Czarnetzki, Novel PtCuO/CeO2/α-Al2O3 sponge catalysts for the preferential oxidation of CO (PROX) prepared by means of supercritical fluid reactive deposition (SFRD). J. Catal. **286**, 78–87 (2012). https://doi.org/10.1016/j.jcat.2011.10.017
144. E.S. Gnanakumar, J.M. Naik, M. Manikandan, T. Raja, C.S. Gopinath, Role of nanointerfaces in Cu- and Cu+ Au-based near-ambient-temperature CO oxidation catalysts. ChemCatChem **6**, 3116–3124 (2014). https://doi.org/10.1002/cctc.201402581
145. X. Liao, W. Chu, X. Dai, V. Pitchon, Bimetallic Au-Cu supported on ceria for PROX reaction: effects of Cu/Au atomic ratios and thermal pretreatments. Appl. Catal. B Environ. **142–143**, 25–37 (2013). https://doi.org/10.1016/j.apcatb.2013.05.010
146. L. Zhang, H.Y. Kim, G. Henkelman, CO oxidation at the Au-Cu interface of bimetallic nanoclusters supported on CeO2(111). J. Phys. Chem. Lett. **4**, 2943–2947 (2013). https://doi.org/10.1021/jz401524d
147. D.I. Potemkin, E.Y. Semitut, Y.V. Shubin, P.E. Plyusnin, P.V. Snytnikov, E.V. Makotchenko, D.Y. Osadchii, D.A. Svintsitskiy, S.A. Venyaminov, S.V. Korenev, V.A. Sobyanin, Silica, alumina and ceria supported Au-Cu nanoparticles prepared via the decomposition of [Au(en)2]2[Cu(C2O 4)2]3·8H2O single-source precursor: synthesis, characterization

and catalytic performance in CO PROX. Catal. Today **235**, 103–111 (2014). https://doi.org/10.1016/j.cattod.2014.04.026
148. J. Papavasiliou, Interaction of atomically dispersed gold with hydrothermally prepared copper-cerium oxide for preferential CO oxidation reaction. Catal. Today (2019). https://doi.org/10.1016/j.cattod.2019.02.026
149. A.A. Firsova, A.N. Il'ichev, T.I. Khomenko, L.V. Gorobinskii, Y.V. Maksimov, I.P. Suzdalev, V.N. Korchak, Selective oxidation of CO in the presence of hydrogen on CuO/CeO2 catalysts modified with Fe and Ni oxides. Kinet. Catal. **48**, 282–291 (2007). https://doi.org/10.1134/s0023158407020139
150. K. Sirichaiprasert, A. Luengnaruemitchai, S. Pongstabodee, Selective oxidation of CO to CO2 over Cu-Ce-Fe-O composite-oxide catalyst in hydrogen feed stream. Int. J. Hydrog. Energy **32**, 915–926 (2007). https://doi.org/10.1016/j.ijhydene.2006.10.060
151. S. Ma, G. Lu, Y. Shen, Y. Guo, Y. Wang, Y. Guo, Effect of Fe doping on the catalytic performance of CuO-CeO2 for low temperature CO oxidation. Cat. Sci. Technol. **1**, 669–674 (2011). https://doi.org/10.1039/c1cy00049g
152. Z. Lendzion-Bielun, M.M. Bettahar, S. Monteverdi, Fe-promoted CuO/CeO2 catalyst: structural characterization and CO oxidation activity. Catal. Commun. **11**, 1137–1142 (2010). https://doi.org/10.1016/j.catcom.2010.05.017
153. H. Bao, X. Chen, J. Fang, Z. Jiang, W. Huang, Structure-activity relation of Fe2O3-CeO2 composite catalysts in CO oxidation. Catal. Letters **125**, 160–167 (2008). https://doi.org/10.1007/s10562-008-9540-3
154. G. Landi, A. Di Benedetto, S. Colussi, P.S. Barbato, L. Lisi, Effect of carbon dioxide and water on the performances of an iron-promoted copper/ceria catalyst for CO preferential oxidation in H<inf>2</inf>−rich streams. Int. J. Hydrog. Energy **41**, 7332–7341 (2016). https://doi.org/10.1016/j.ijhydene.2016.03.141
155. V.D.B.C. Dasireddy, B. Likozar, J. Valand, Preferential oxidation of CO in H2/H2O/CO2 water–gas shift feedstocks over Cu-based carbon nanotubes-supported heterogeneous catalysts. Appl. Catal. B Environ. **237**, 1044–1058 (2018). https://doi.org/10.1016/j.apcatb.2018.06.069
156. J. Wang, C. Han, X. Gao, J. Lu, G. Wan, D. He, R. Chen, K. Chen, S. He, Y. Luo, Rapid synthesis of Fe-doped CuO-Ce0.8Zr0.2O2 catalysts for CO preferential oxidation in H2-rich streams: effect of iron source and the ratio of Fe/Cu. J. Power Sources **343**, 437–445 (2017). https://doi.org/10.1016/j.jpowsour.2017.01.084
157. Z. Liu, R. Zhou, X. Zheng, Influence of residual K+ on the catalytic performance of CuO - CeO2 catalysts in preferential oxidation of CO in excess hydrogen. Int. J. Hydrog. Energy **33**, 791–796 (2008). https://doi.org/10.1016/j.ijhydene.2007.10.011
158. A.B. Dongil, B. Bachiller-Baeza, E. Castillejos, N. Escalona, A. Guerrero-Ruiz, I. Rodríguez-Ramos, Promoter effect of alkalis on CuO/CeO2/carbon nanotubes systems for the PROx reaction. Catal. Today **301**, 141–146 (2018). https://doi.org/10.1016/j.cattod.2017.03.033